

Recent advances in effect of crystallization dynamics process on the morphology of active layer in organic solar cells

Qiuju Liang¹, Mingzhi Duan², Xingpeng Liu², Haolei Zhu², Kaiqi Yang², Wen Zhang²,
Jingming Xin², and Jiangang Liu²

¹Northwestern Polytechnical University

²Affiliation not available

March 12, 2024

Abstract

Organic solar cells (OSCs) have received widespread attention due to light weight, low cost, semitransparency and ease of solution processing. By continuously improving materials design, active layer morphology, and device fabrication techniques, the power conversion efficiency (PCE) of OSCs have exceeded 20%. The morphology of the active layer, which includes the phase separation structure, the degree of crystallinity of molecules, and the domain sizes, plays a critically important role in the performance, which is significantly influenced by the crystallization dynamics of the donor and acceptor. Therefore, it is crucial to comprehensively understand how the dynamics impact the film structure and how to effectively employ the kinetic procedure to enhance the structure of the active layer in OSCs. In this review, the methods and principles of kinetics characterization were introduced. Afterwards, the latest advancements in the control of film-forming and the post annealing process are outlined, unveiling the underlying mechanism. In conclusion, the potential and future of OSCs were anticipated and projected. Researchers may gain a comprehensive comprehension of how the dynamic process affects the morphology through this review, potentially enhancing the performance of OSCs.

1 Introduction

Organic solar cells (OSCs) have developed rapidly due to low cost, light weight, semitransparency, solution processability and so on, which have become one of the most dynamic research frontiers in the field of new materials and new energy.[1-9] At present, the power conversion efficiency (PCE) of OSCs has exceeded 20%.[10] In order to improve the PCE, researchers have made numerous efforts in optimization of material design, device structure and morphology of the active layer, etc.[1, 11-16]

The energy conversion process of OSCs mainly includes the following steps: photon absorption, diffusion of excitons, charge transfer state (CT state) separation, transport of charge and collection.[17-23] Through in-depth understanding of the working principle of OSCs, it is obvious that the film morphology of the active layer formed by the mixed donor and acceptor materials plays a decisive role in the effective separation of excitons and carrier transport.[24-26] To ensure the PCE of OSCs, the ideal morphology should have the following characteristics: (1) The bicontinuous phase separation structure: both donor and acceptor materials form a continuous pathway to ensure that carriers can be efficiently transmitted to the corresponding electrode and collected.[27-29] Simultaneously, it is necessary to ensure that the excitons diffuse to the donor/acceptor (D/A) interface within the lifetime by maintaining domain sizes of 10-20 nm.[30-34] (2) High degree of crystallinity: a significant level of crystallinity in the active layer molecules is advantageous for charge transfer as it allows carriers to move along the primary chain and interchain via the π - π stacking of molecules.[35-42] (3) Simultaneous face-on orientation: the face-on orientation enhances the vertical carrier transport within the active layer.[43-45] Furthermore, the same molecular orientation at the interface

between the donor/acceptor promotes the separation of charge transfer states.[46-53] Therefore, the morphology of the active layer significantly influences the photophysical process and subsequently the PCE. The morphology is seriously affected by crystallization dynamics in the fabrication process of active layer, which mainly happens in the film-forming and post annealing process.[25]

Film-forming kinetics refer to the physical laws and dynamic processes that organic semiconductor materials follow during the formation of a film. In the initial stage of film-forming, the molecular clusters begin to nucleate, and then grow and form aggregates. Because of the influences of van der Waals interactions, hydrogen bonds, and π - π stacking interactions, these aggregates constantly change their size, shape, and orientation. As the concentration of the solution and the number of aggregates increase further, they are separated from the solution, forming liquid-liquid (L-L) or solid-liquid (S-L) separation. In solid-liquid phase separation, the clusters are deposited on the solid surface, forming a continuous film. In L-L separation, the clusters form discrete droplets that self-assemble into continuous films, usually under surface tension. Subsequently, the crystal continuously adsorbs organic molecules on the crystal surface, the volume increases with the increase of time, and eventually tends to mature. Since Heeger A.J. et al. invented OSCs with bulk heterostructure in 1995[54], researchers have carried out a lot of work to optimize the morphology of the active layer, and developed strategies such as solution state and post-annealing treatment to control the active layer morphology. During the solution treatment process, the morphology is affected by many factors, including solvent selection, temperature, deposition method, and the use of additives.[55] Therefore, understanding and optimizing these processes is critical in developing high-performance OSCs.

In addition, post-treatment processes, such as thermal annealing (TA) and solvent vapor annealing (SVA), can also optimize the morphology of the active layer. TA is an effective means to adjust the morphology of active layers in blends. Since Friend et al. first found that TA can improve the performance of P3HT:EP-PTC blends, TA has officially entered the field of regulation of active layer in OSCs.[56] The main principle of TA is that the polymer is heated above the glass transition temperature (T_g) to promote the movement of polymer chain segments, so as to achieve the ordered aggregates of polymer molecules. At the same time, the molecules are diffused and crystallized during the annealing process, and finally form the interpenetrating network structure.[57, 58] For SVA, the blend film is placed in solvent vapor. After the solvent molecules penetrate into the active layer, the polymer chains are induced to reassemble into an ordered structure.[59, 60] For example, Yang et al. made the P3HT:PCBM blend film dry slowly through dichlorobenzene solvent vapor, so that the blend film self-assembled to form an ordered structure and good phase separation morphology, which is conducive to the balance of electron and hole mobility.[61]

This review focuses on the effect of crystallization dynamics on the morphology of OSCs and reveals its potential mechanisms of how it influencing the morphology. Firstly, the characterization methods and kinetic principles of the thin films are briefly described. Subsequently, the common strategies for the morphology optimization of OSCs active layers, including adjusting the film-forming process and the post-treatment process are summarized, and the typical examples are cited to understand how these treatments affect crystallization dynamics process to achieve the desired morphology. Finally, the future development of OSCs was prospected, which may provide some guidance for achieving high PCE of OSCs.

2 Characterization of the crystallization kinetics

As we discussed above, intensively structure evolution occurs during film-forming process and post-treatment process, which determines the final morphology of the active layer. Therefore, monitoring structure evolution is conducive to analyze the crystallization kinetics. In situ characterizations are powerful tools to extract real-time structural information, where the in situ optical spectrum and X-ray scattering are frequently utilized with customized film-forming setup. In the following paragraph, we briefly summarize various common measurements, such as ultraviolet visible absorption spectroscopy (UV-vis) absorption spectra, photoluminescence (PL), grazing-incidence wide-angle X-ray scattering (GIWAXS), and grazing incidence small-angle X-ray scattering (GISAXS). Then, we emphasize their significance and refer to classic examples to elucidate the information derived from each in situ characterization technique.

2.1 The in situ UV-vis absorption spectrum

In situ UV-vis is an analytical technique used to monitor and study chemical reactions, material transformations, and changes in optical properties, which can be used to characterize the absorption spectrum of organic semiconductor. The change of peak shape of absorption spectrum often reflects the change of its aggregation form.[62-64] For example, the extension of conjugation produces redshifts, and the increase in aggregates homogeneity results in sharper peaks or shoulders.[65] In addition, the change of absorbance of a certain wavelength can also be measured to study the film crystallization kinetics.[66] Figure 1a illustrates the schematic diagram of the in situ UV-vis absorption.[67] Shen et al. used in situ UV-visible spectroscopy to investigate the effect of different temperatures on the film-forming rate of the PM6:Qx-1 blend system. In the first stage, the peak position of Qx-1 at 718 nm showed no significant change during the solvent evaporation process. During the second phase, there was a rapid red-shift (830 nm) in the absorption peak of Qx-1. As the temperature increased, the second stage duration decreased from 6.50 s at 40 °C, to 5.52 s at 60 °C, 3.36 s at 80 °C, and finally 2.74 s at 100 °C. The position of the absorption peak for Qx-1 started to redshift, suggesting gradual acceptor aggregation and crystallization. The absorption peak of PM6 did not change significantly (600 nm). In the third stage, the Qx-1 absorption peak reached a constant position with no significant changes. Yu et al. studied the relationship between PTB7 molecular chain length and its aggregation state by using UV-vis absorption spectroscopy.[68] With a low number of monomer units (1.5), the solution's absorption peak is primarily focused around 500 nm, but as the number of monomer units increases (3.5), the absorption peak gradually shifts towards 570 nm. As the number of monomer units increases, the level of conjugation within the molecular chain also increases, which reduces the energy difference between energy levels and causing a spectral redshift.

2.2 The in situ PL spectrum

The PL spectrum can reflect the phase separation process of solvent volatilization through changes in fluorescence efficiency and luminescence peak position.[69] With the evaporation of solvent, the degree of aggregation and cluster formation will gradually increase, which will lead to the increase of fluorescence efficiency.[70] Furthermore, the interaction between organic molecules will gradually strengthen due to the formation of aggregates and clusters, which will lead to the redshift of fluorescence peak position.[71] When the phase separation reaches a certain degree, the fluorescence efficiency will reach the maximum value, and the fluorescence peak position will also reach a stable state. While in situ photoluminescence (PL) measurements are relatively straightforward to conduct, it is crucial to exercise caution when analyzing the data. The reason for PL quenching during the drying of BHJ blends is the result of various molecular interactions, such as photochemical oxidation, reactions in the excited state, rearrangement of molecules, transfer of energy, and the creation of complexes in the ground state.[72] To fully utilize the in situ PL spectrum for BHJ drying, it is necessary to elucidate the mechanism of PL quenching during the drying process.[73] The experimental equipment is shown in Figure 1b. Engmann et al. studied the film-forming process of P3HT:PCBM blends using in situ PL.[74] During the early phase, the PL intensity of P3HT diminishes as the mean separation between evenly dispersed fluorophores and quencher molecules decreases. In the second stage, PL intensity of P3HT drops sharply and then recovers. The abrupt decline in PL is ascribed to a prolonged exciton diffusion distance, enabling reach to quenchers situated at greater distances, subsequently leading to domain coarsening that ultimately leads to the restoration of PL. In the third stage, the PL decreases, and the emission ratio continues to increase. The emission intensity of ordered polymer domains primarily determines the overall PL, while fluorescence from the disordered phase is greatly reduced. Huang et al. studied P3HT spectra at different concentrations.[75] When the concentration is low, the PL peak position is 570 nm. When the concentration increases, the peak strength increases, indicating that P3HT is a single-chain state. When the concentration rose to 0.02%, PL intensity decreased sharply with the increase of concentration. This is because the P3HT molecules come into contact, causing the fluorescence to be quenched and the intensity to decrease. When the concentration was 1%, new peaks appeared at 640 nm and 670 nm. This is because the molecules are π - π stacking, forming ordered aggregates, and the energy of the system is reduced.

2.3 The in situ GIWAXS and GISAXS

GIWAXS, is based on scattering X-rays to study the molecular arrangement and crystal structure of a sample. GIWAXS detector is close to the sample, the scattering angle range detected is large, and the corresponding q value is large. According to $d = 2\pi/q$, it can be seen that the detected crystal plane spacing is small. Therefore, GIWAXS represents the crystallization and ordered arrangement of molecular scale.[76-78] For example, the aggregation state of organic semiconductor molecules and the evolution of crystal structure in solution can be monitored in real time by in situ GIWAXS. By monitoring the change of diffraction pattern, the growth rate of crystal, molecular orientation and the optimization of crystal structure can be revealed. Perez used in situ GIWAXS to study the effect of DIO on the p -DTS(FBTTh₂)₂:PCBM films.[79] If no DIO is added, p -DTS(FBTTh₂)₂ crystallinity is low. When DIO is used, p -DTS(FBTTh₂)₂ first forms an intermediate phase (liquid crystal phase) in the film, and then the liquid crystal phase gradually transforms into a crystalline phase in the middle and late stages of film-forming, and the crystallinity of the film is improved. The scattering data for the sample treated with the additive reveals multiple distinct and intense peaks. The peaks' sharpness, combined with the emergence of higher-order reflections at q [?] 5.6 and 8.4 nm⁻¹, show that the correlation length and quality of the crystals in the film treated with the additive are significantly improved. GISAXS can characterize the long-period structure, quasi-periodic structure and interfacial layer structure on a larger scale. GISAXS detector is far away from the sample, has a small range of detected scattering angles, a small corresponding q value, and a large distance between detected crystal faces. Therefore, GISAXS represents the ordered arrangement of phases and aggregates. Figure 1c shows the schematic diagram of GIWAXS and GISAXS. Russell et al. used GIWAXS and GISAXS to study the role of DCB in DPPBT:PC₇₁BM film.[80] The change of intensity of peak (100) in GIWAXS of the DPPBT can explain the change of crystallinity. In addition, the change of scattering peak location in GISAXS can explain the degree of phase separation. The results show that when DCB content is 5%, the (100) peak intensity of GIWAXS of the DPPBT changes synchronously with the scattering peak position of GISAXS. When the DCB content is high (20% and 50%), the (100) peak intensity of GIWAXS increases earlier than the shift of GISAXS scattering peak location, indicating the crystallization signal of GIWAXS changes before the phase separation signal of GISAXS. This indicates that DCB promotes the crystallization of DPPBT.

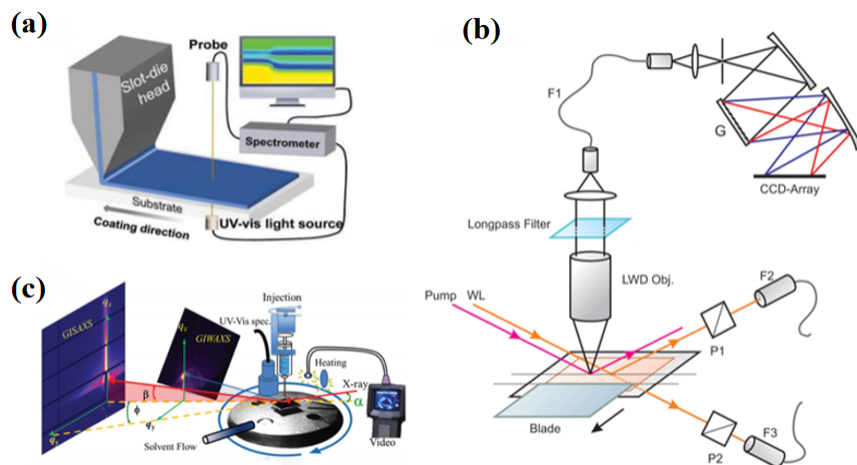


Figure 1. (a) In situ UV-vis absorption measurement device schematic illustration. Reproduced from [67]. (b) Schematic diagram of in situ PL experimental facility. Reproduced from [74]. (c) Schematic illustration of in situ GISAXS/GIWAXS measurements device. Reproduced from [81].

The above several in-situ characterization methods are more commonly used techniques, which can well characterize the evolution of thin films, facilitate us to better understand the crystallization dynamics, and then find regulatory means to optimize the morphology. The principles of film-forming dynamics and the

regulation of film-forming and post-annealing processes will be introduced next.

3 Regulation principle of the film-forming kinetics

The kinetics can influence the morphology and properties. In the solution processing, the nucleation, crystallization and crystal growth occurs with the solvent volatilization, which is coupled with the phase separation process, making the process more complex.

In the solution processing, the initial state is the dissolved state. The process of dissolution is the dispersion of molecules into solution by solvent. And dissolution rate is related to molecular diffusion, reaction activation energy, surface energy and other factors. It can be calculated by Fick's law, that is, the dissolution rate is proportional to the concentration, which can be described by the following formula:[82]

$$\frac{\partial C}{\partial t} = D \frac{\partial^2 C}{\partial x^2} \quad (1)$$

Where C is the concentration of the substance in the solution, t is the time, x is the spatial coordinate, and D is the diffusion coefficient.

As the concentration starts to increase, the solution starts to nucleate. The nucleation rate can be expressed by the following formula:[83, 84]

$$\text{rate} \propto D(T) \bullet \exp\left(-\frac{W^*}{kT}\right) \quad (2)$$

$D(T)$ represents the diffusion coefficient while W^* denotes the energy expended in the creation of a nucleus with the minimum required size. Determining a molecule's ability to participate in nucleation is heavily influenced by the diffusion coefficient. Viscosity is inversely proportional to η , as stated by the Stokes-Einstein relation. An equation of the Vogel-Fulcher-Tammann type effectively describes the exponential increase in the diffusion coefficient when $T - T_g$ is less than 100 °C:[85]

$$D(T) \propto \exp\left(\frac{-B}{T-T_0}\right) \quad (3)$$

both B and T_0 are constants.

To form the critical size nucleus, energy input is necessary to balance the following two aspects: (1) the volume free energy difference between the liquid and crystalline states, $G_{1c} = G_1 - G_c$, (2) the interfacial energy γ_{1c} is related to the surface of the nucleus.

As the degree of undercooling increases, the energy barrier for uniform nucleation indeed decreases, making it easier for nucleation to occur in supercooled liquids. On the other hand, in the event of heterogeneous nucleation, the formation of the nucleus occurs on an existing solid surface, there is a notable decrease in the energy barrier for nucleation. This reduction in the energy barrier facilitates and accelerates the nucleation process.

Various factors, including the volatility of the solvent, spinning speed, and the temperature of the solution and substrate, determine the rate of solvent removal from the upper layer.[82] The initially dilute solution becomes enriched in both solutes as the solvent is depleted. This enrichment leads to increased interaction between the solutes and leads to morphology evolutions. When the solvent is extracted, the mixture enters the spinodal range, leading to phase separation. As the solvent is depleted, the solution begins to be rich in these two solutes. The interaction between solutes will increase and the morphology will change. As the solvent is removed, the mixture reaches the spinodal region (immiscible conditions), resulting in the phase separation.[86] Under these conditions, the resolution becomes precarious, and even slight variations lead to rapid separation of phases. In general, the solution is divided into two phases enriched with donor and acceptor, respectively. Following these two initial formation stages, there is a subsequent slow coarsening process. The rate at which the solvent is removed affects the kinetics of phase separation and coarsening.[82]

The crystal growth rate is given in the following format:[84]

$$\text{rate} \propto D'(T) \bullet [1 - \exp\left(-\frac{G_k}{kT}\right)] \quad (4)$$

The crystal growth involves long range diffusion, while nucleation only requires particles to diffuse over a short distance near the interface between the crystal and the melt.[87]

Typically, the maximum rates of nucleation and crystal growth occur near T_g and T_m , respectively. To achieve crystallization, it is necessary to have nucleation and the growth of crystals at a decent speed. Hence, the extent of intersection between nucleation and crystal growth regime plays a crucial role in determining if crystallization takes place in the molten state while undergoing cooling. The highest rate of crystallization takes place within the temperature range of T_g and T_m . Alternatively, the process of crystallization can be initiated by initially subjecting the material to annealing at a temperature in proximity to T_g , and subsequently conducting a second annealing phase at a temperature nearer to T_m , which promotes accelerated growth of crystals.[85]

Crystal growth is also affected by many factors, such as temperature, additives, molecular interactions, and so on. With the complete evaporation of solvent, the crystal structure tends to be stable, and the film-forming process is basically completed. Finally, through the interaction of these dynamic processes, the final morphology of the organic solar cell film is formed if there is no post annealing process.

In summary, understanding the film-forming process in detail is crucial for investigating the thermodynamics and kinetics of thin film drying and optimizing the morphology of the active layer to achieve high device performance. Schmidt Hansberg et al. utilized in situ GIWAXS to reveal the kinetics and thermodynamics of molecular ordering during the thin film drying process, which deepened the understanding of the film-forming process.[31] In the initial stage, the DCB content was only 3 wt%, and as the solvent gradually evaporated, the DCB content increased to 14 wt%. As DCB gradually evaporated, PCBM reached its maximum solubility first, while P3HT transitioned from the solution state to the gel state. The stacking signal of the P3HT side chains in the out-of-plane direction (100) increased, but the aggregation diffraction peak of PCBM appeared only after the ordering of P3HT, indicating that the interaction between the polymer and the fullerene inhibited the aggregation and clustering of the fullerene molecules, leading to the formation of clusters in the final stage of thin film drying after complete stacking of P3HT molecules. As the solvent further evaporated, P3HT crystallization became more complete, and PCBM entered the amorphous region of P3HT, aggregating to form clusters.

The morphology of thin films significantly influences photoelectric properties like charge transfer and energy transfer. It's important to recognize that the actual dynamics of film-forming are highly intricate. Therefore, further theoretical models and experimental investigations are required to delve deeper into these processes.

4 Regulation of film-forming process

As aforementioned, film forming is a complicated process involving multiple physical processes. Here we introduce the method of optimizing the morphology, including the film-forming method, solvent, temperature and additives.

4.1 Film deposition methods

The morphology can be significantly influenced by the deposition method used to film processing.[88] Different deposition methods, generally including spin-coating, blade-coating and slot-die (Figure 2), can lead to different structures and packing arrangements of the molecules, which can affect the device performance. For example, spin-coating spreads solution on the substrate then quickly shakes off the solution by the centrifugal force, which can form a relatively smooth and uniform film with small crystalline domains.[89] Blade-coating and slot-die use the shear force formed by bending liquid surface to coat the solution on the substrate, which have a certain induction effect on the aggregation and arrangement of solute molecules.[90, 91] In addition, there are some new film-forming methods, such as meniscus-assisted-coating (Figure 2d).

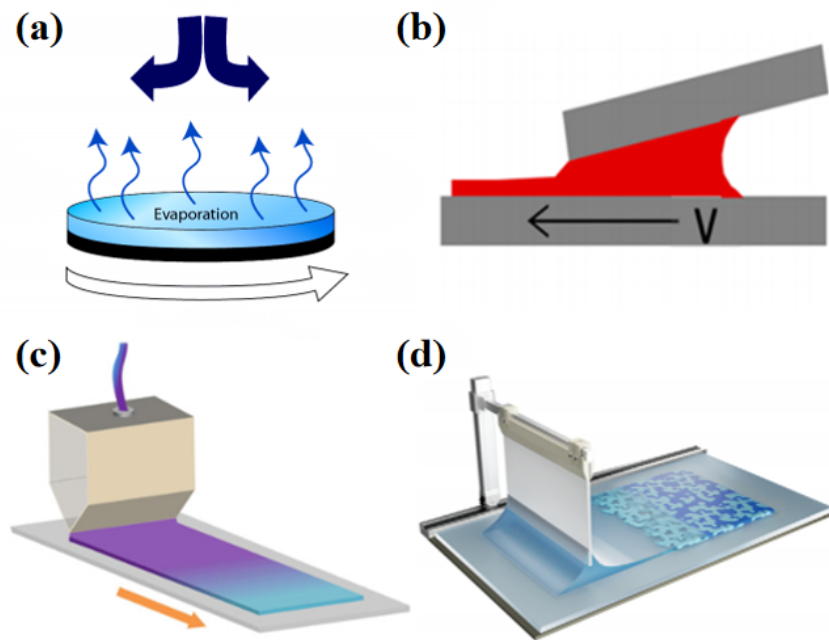


Figure 2. (a) Schematic diagram of spin-coating process. Reproduced from [92]. (b) The blade-coating process is illustrated in a schematic diagram. Reproduced from [65]. (c) Diagram illustrating the structure of slot-die. Reproduced from [93]. (d) Schematic illustration of MAC. Reproduced from [88].

4.1.1 Spin-coating

Due to the ease of use and safety, spin-coating is often used in laboratory. Franeker et al. used a variety of measurement methods to study film-forming process of spin-coating.[89] Figure 3b shows the PS:PC₇₀BM:oxylyene phase diagram calculated with Flory-Huggins theory. Figure 3a shows four stages of the film-forming process, at initial stage, scattered GISAXS strength decreases with the decrease of film thickness. During the commencement of laser scattering ($t = t_{\text{onset}}^{\text{LS}}$), the solution undergoes an internal phase separation, resulting in the formation of domains enriched with PC₇₀BM and PS, which are extensively swollen (average $\varphi_{\text{solv}} = 70\%$). Subsequently, the separation of the L-L phase takes place, and the signal strength increased. The scattering intensity for GISAXS ($t = t_{\text{onset}}^{\text{GISAXS}}$) significantly increases, primarily because o-xylene has a strong attraction to PS, causing the PC₇₀BM-rich domains to have a lower solvent content compared to the PS-rich matrix. Therefore, the PC₇₀BM-rich domains will dry earlier. The peak intensity rapidly increases. Eventually, the solvent evaporates, forming a film. Reichenberger et al. studied the effect of spin-coating on aggregates at a critical temperature T_c . [94] Figure 3c compares the absorption of PCE11 aggregates above and below T_c . When spin-coating at 22 °C, compared to the collective absorption spectrum observed at 70 °C, the collective absorption spectrum exhibits an absorption peak at a slightly reduced energy and has a larger peak ratio of 0-0/0-1. The observed behavior in P3HT is comparable and indicates a stronger delocalization of electronic states throughout the polymer chain. This increased delocalization is accompanied by a reduction in inter-chain coupling. They believe that once the deposited solution approaches T_c in the first few seconds, the molecules form aggregates. In the film, residual solvents persist, and they can assist in generating planarized chromophores with robust intra-chain connection. These planarized chromophores might serve as nuclei in the subsequent transformation process. As a result, for both P3HT and PCE11, spin-coating onto a substrate below T_c doesn't substantially affect the quantity of aggregates formed. However, it does alter the nature or characteristics of these aggregates.

4.1.2 Blade-coating

Compared with spin-coating, blade-coating is more suitable for industrial applications because it is comparable with large area film fabrication.[95] Peng et al. studied the effects of the blade-coating speed and the third component on the film-forming process.[96] When the coating speed increases, the thickness of the film also increases.[97] A relatively prolonged transition process from solution to film may promote an increase in crystallinity. As a result, at a medium speed of 20 mm/s, polymers and small molecules demonstrated appropriate pre-aggregation and underwent a comparatively extended process of crystallization and molecular arrangement. In addition, the introduction of components also changes the film-forming kinetics (Figure 3d). In the first stage, as the solvent evaporates, some polymers or small molecules begin to aggregate in an ordered fashion. During the second phase, the incorporation of the third component hinders the formation of crystal nuclei, leading to the simultaneous crystallization of both the polymer and small molecules. During the third phase, the residual solvent allows for further rearrangement of the polymer chains or small molecules, leading to the achievement of optimal crystallization. Stage four, the drying process is complete. As a result, the ternary membrane exhibits a greater degree of molecular organization and a reduced size of phase separation. In addition, appropriate sequential deposition process methods can also improve the crystallization of donor/acceptor. Wang et al. deposited PBDB-T:FOIC onto PBDB-T:IT-M films by sequential-blade cast (seq-blade cast), thereby improving donor and acceptor crystallization.[90] The seq-blade cast method can induce varying levels of dissolution, blending, and phase separation between the upper and lower layers. This phenomenon facilitates the efficient mixing of the donor and acceptor components to obtain more ideal nanostructures and morphologies. The PBDB-T:FOIC in the seq-blade cast system creates a fresh structure, and the PBDB-T:IT-M bottom layer supplies numerous crystal nuclei. The competitive process of growth encouraged the formation of PBDB-T crystals and restricted the clustering of FOIC, resulting in minimal phase separation in the film. The binary films take a relatively long time to crystallize, approximately 18 seconds, whereas the PBDB-T:IT-M layer and PBDB-T:FOIC layer of seq-blade cast films reach their peak at 14 seconds and 8 seconds, respectively (Figure 3e). In the case of seq-blade cast film (Figure 3f), the PBDB-T aggregation rate rose from 0.0428 to 0.0574. The results show that the seq-blade device demonstrates the highest OSC performance, with a PCE of 11.91%. Yuan et al. studied the film-forming dynamics of patterned blade coating.[98] The use of micro-structured pattern printing blades allows for the adjustment of flow conditions to enhance the alignment of molecules and facilitate mass transfer in the crystallization process. The fluid can be facilitated to have both extensional and shear flow simultaneously by these arrays of micro-structured blades. Experimental evidence has demonstrated that extensional flow can align conjugated polymer chains, while shear flow has the potential to induce elongation and modify the structure of these polymers. During the subsequent evaporation process, the tight packing and arrangement of PM6 polymer chains, influenced by both extensional and shear flow, leads to effective crystallization of Y6 molecules. As shown in Figure 3g and h, among the four films, the film prepared with a low-speed patterning blade (PBC-LS) has the highest CCL, indicating excellent crystallinity. Simultaneously, PBC-LS films exhibit a smaller π - π stack distance of 0.36 nm and a lamellar stack distance of 2.1 nm, suggesting a molecular structure that is densely packed. These films demonstrate superior crystallinity and well-defined phase separation, which is attributed to the patterned blade's ability to minimize disturbances of the solution. Finally, the PCE of PM6: Y6 film prepared by PBC-LS was 15.93%, while the PCE of ordinary blade was 14.55%.

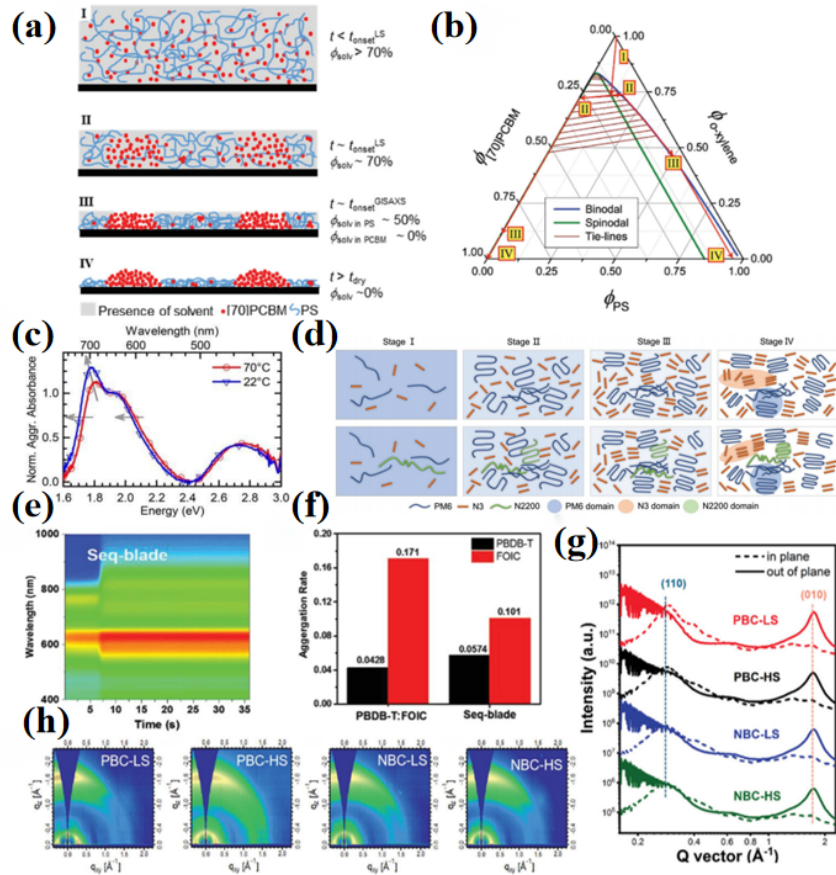


Figure 3. (a) Diagram illustrates the formation of the PC₇₀BM domain through spinodal demixing. Reproduced from [89]. (b) The Flory-Huggins theory was used to calculate the phase diagram of PS:PC₇₀BM:oxylene. Reproduced from [89]. (c) Aggregate absorption spectra were recorded for a PCE11 film after spin-coating at both 70°C and 22°C, with normalization at 1.94 eV. Reproduced from [94]. (d) The morphology-forming process for films made of polymer:nonfullerene small molecules and polymer:nonfullerene small molecule:polymer blends is schematically depicted. Reproduced from [96]. (e) Absorption patterns of seq-blade cast films in two dimensions. Reproduced from [90]. (f) Relative rate of aggregation for PBDB-T and FOIC. Reproduced from [90]. (g) Corresponding 1D GIWAXS line profiles. Reproduced from [98]. (h) 2D GIWAXS data of PM6:Y6 blend films. Reproduced from [98].

4.1.3 Slot-die coating

Slot-die coating involves delivering a solution onto a substrate through a narrow slot situated in close proximity to the surface. Slot-die coating offers a greater advantage over spin-coating due to its superior efficiency in material conservation. Zhao et al. studied the film-forming kinetics of slot-die by introducing the third component.[91] Kinetic studies have unveiled that improved miscibility between BTR-Cl and D18 plays a pivotal role in the segregation of Y6 from the mixed phase with D18. Additionally, the presence of highly crystalline BTR-Cl accelerates the L-L phase separation of the D18:Y6 mixture, leading to a greater accumulation of Y6 molecules. The Y6 peak location redshift in the D18:BTR-Cl:Y6 blend shifts noticeably earlier compared to the D18:Y6 blend, as depicted in Figure 4a. This observation suggests that Y6 tends to aggregate more quickly. In 110 nm and 300 nm thick photoactive films, PCE reached 17.2% and 15.5%, respectively. The use of slot-die coating in conjunction with a ternary design approach has demonstrated its effectiveness in manufacturing thick, large-scale, and flexible OSCs with high efficiency. The utilization

of industry-scale R2R fabrication techniques showcases the replicability of outcomes with this approach. Zhao et al. developed a sequential slot-die (SSD) coating method for the preparation of OSCs at room temperature using halogen-free solvents.[99] The device was prepared in ternary systems with PTB7-Th and *p*-DTS-(FBTTH₂)₂ as donors and PC₇₁BM as acceptors. In the SSD coating process, PTB7-Th is used as the first coating. In fact, PTB7-Th molecules undergo two phases of aggregation (Figure 4b). The solvent from the second layer has the ability to dissolve some of the PTB7-Th molecules. During PCBM fabrication, these dissolved molecules move to the upper surface and reassemble into aggregates. Furthermore, when the polymer is coated with the first layer, the size of the area gradually expands, resulting in an appropriate phase separation. The power conversion efficiency (PCE) of devices produced using SSD coating is improved from 6.09 to 7.32%, indicating a 20% increase in PCE.

4.1.4 Other film-forming methods

In addition to the deposition methods above mentioned, meniscus-assisted-coating (MAC) are also effective strategies. The meniscus coating is done by pumping paint into the applicator roller. The paint flows through the porous surface of the applicator roll, forming a film on the substrate that is transported by the coating roller. The configuration and dimensions of the meniscus established within the gap between the rollers are influenced by variables such as the gap distance, the speed, and the rotational direction of the rollers.[100-103] Different flow regions will be formed inside the liquid, and coating speed and temperature have significant effects on the formation of film thickness. Yue et al. used MAC strategy to prepare a PM6:PY-IT film with high crystallinity and nano interpenetrating networks.[88] As shown in Figure 4c, the researchers investigated the crystallization kinetics of the polymer blend film. The results revealed a straightforward linear correlation between the rate of meniscus movement and the extent of crystallinity in the polymer. With the increase of V_a , the absorption peak intensity of PM6 and PY-IT decreased significantly, indicating that the crystallinity of the blend film decreased with the increase of V_a . But when the speed is reduced to 1 mm/s, it leads to excessive crystallization of the polymer. The results show that by using MAC strategy and precisely controlling the propulsion rate, the active layer can obtain finer nanofiber networks. In the end, the PCE exceeded 15%.

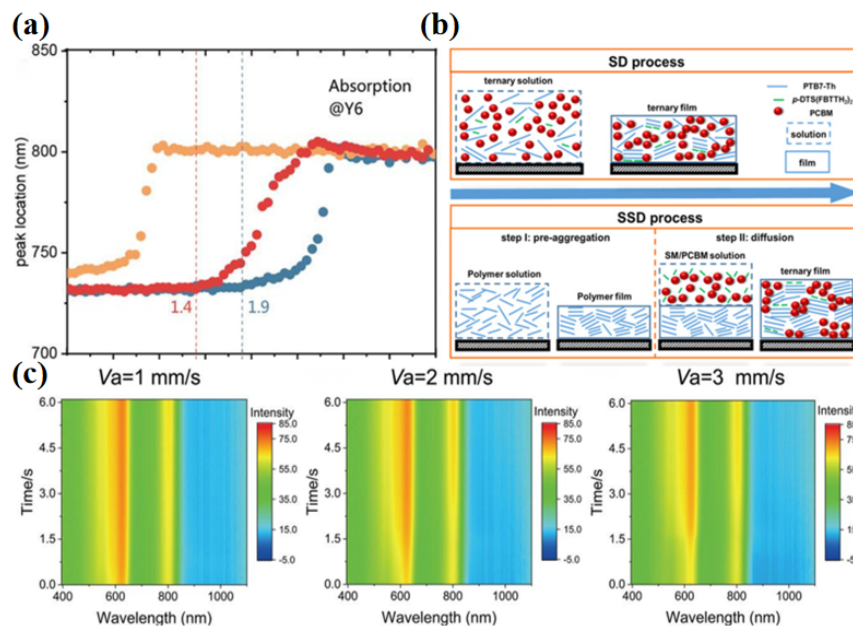


Figure 4. (a) The temporal progression of the peak location of Y6. Reproduced from [91]. (b) Schematic diagram illustrating the pre-aggregation process in the SSD method. Reproduced from [99]. (c) In situ

UV-vis absorption spectra during MAC preparation. Reproduced from [88].

4.2 Selecting the processing solvent

Different solvents have different effects on the interaction between polymer and small molecules, solvent volatilization rate and molecular diffusion rate, which results in different morphologies. Generally, there are many interaction forces between solvent and solute, including van der Waals force, electrostatic interaction, hydrogen bond, etc., which can stretch and contract polymer chain, or stabilize polymer chain structure, thus changing the structure and arrangement of crystal. Strong solvent-polymer interactions contribute to the formation of interspersed nanonetwork structures, while weak interactions tend to lead to the formation of condensed phases. In addition, the choice of solvents also needs to consider its environmental protection and cost. Therefore, these factors should be considered comprehensively when optimizing the morphology of active layer.

The specific solvents can shorten film-forming times, which can prevent the larger phase separation structure caused by high crystallinity. Zhu et al. replaced CB with 2-methyltetrahydrofuran (MTHF) to shorten the film-forming time of PTzBI-Si: N2200 blend film from 11.7 s CB to 3.7 s.[104] Due to the low boiling point of MTHF, the solution evaporates quickly, which can greatly shorten the film formation time. The shortened film-forming time leads to a decrease in crystallinity, which inhibits the formation of large-scale structures. And the diameter of PTzBI-Si crystal is reduced from 400 nm to 35 nm (Figure 5a). The smaller phase separation structure enhances exciton dissociation, leading to increase the J_{sc} from 2.76 mA cm⁻² to 15.41 mA cm⁻² and resulting in an increase in PCE from 1.01% to 9.01%. Rational use of mixed solvents can also promote vertical phase separation. Sun et al. used chlorobenzene/tetralin to prepare P3HT:PCBM films to regulate the film-forming process.[105] During film formation, chlorobenzene evaporates rapidly, leaving tetralin with a high boiling point in the film. Since PCBM has a much better solubility than P3HT, most PCBM dissolve in tetralin, while P3HT begins to precipitate. At the later stage of film formation, the slow evaporation rate of tetrahydronaphthalene prolonged the film-forming time, PCBM molecules have more time to move and can diffuse upward with tetralin evaporation. Based on the X-ray photoelectron spectroscopy results (Figure 5b), the PCBM to P3HT quality ratio (mPCBM:mP3HT) experienced an increase from 0.1 to 0.72 in close proximity to the film surface, consequently leading to the formation of a vertical phase separation structure. The PCE is 1.5 times better than that of devices without tetralin.

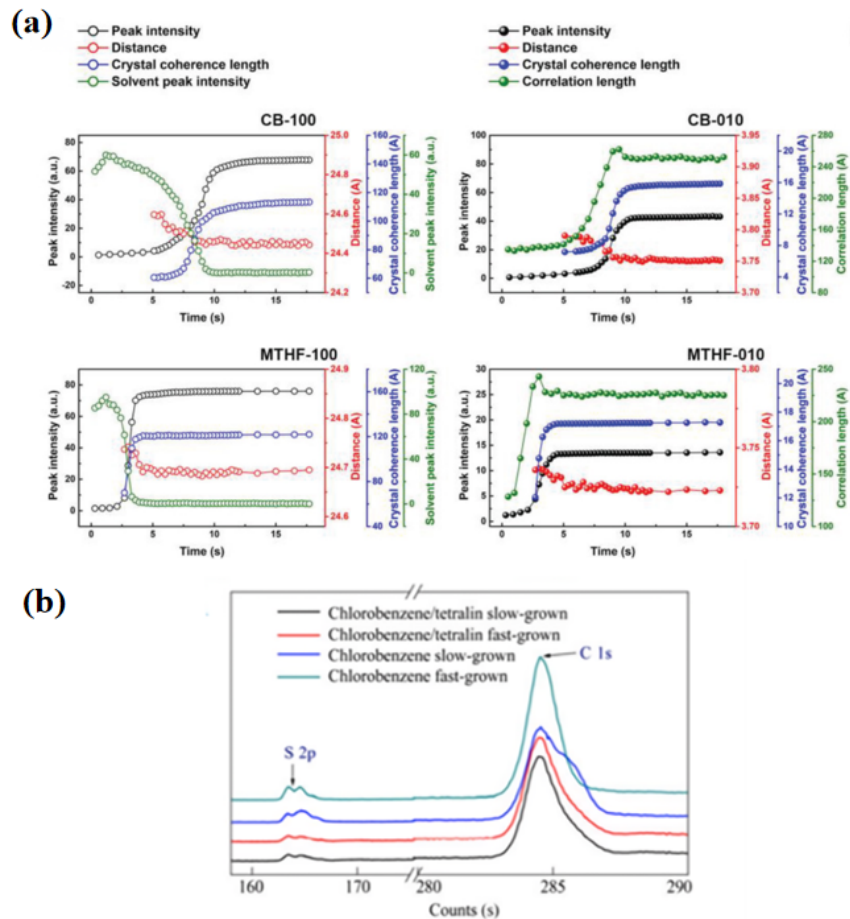


Figure 5. (a) Analysis of in situ GIXD results. Peak fitting was employed for the (100) and (010) peaks to determine various parameters. Reproduced from [104]. (b) Spectra of X-ray photoelectron spectroscopy (XPS). Reproduced from [105].

The appropriate solvent can change the crystallization of molecules and the aggregation state of the solution. Jiang et al. used CF instead of CB to balance the crystallization of molecules in PDTBT2T-FTBDT:BTP-4F blends.[106] They observed that PDTBT2T-FTBDT exhibited a tendency to primarily form H-aggregates in the solvent, while BTP-4F had a preference for forming J-aggregates. The subpar performance of devices coated using slot-die printing with CB can be ascribed to the excessive J-aggregation of BTP-4F, which leads to an imbalance in donor and acceptor crystals and a less ordered molecular alignment. After the addition of CF, the aggregation of BTP-4F was inhibited, and the crystallization was more balanced. As shown in Figure 6a-d, with the passage of time, the number of face-on oriented molecules in the blend film added with CF gradually exceeds the number of isotropic molecules, which does not exist in CB. Compared with CB blending films, the blending films using CF have better morphology, smoother surface and more obvious crystal orientation. In the end, the PCE increased to 13.2%. Zhou et al. changed the solvent from CN and o-DCB to CB, successfully changing the orientation of the P(NDI2OD-T2) molecules.[107] When CB is used instead of CN, the molecular orientation of P(NDI2OD-T2) will change to face-on (Figure 6e, f). This is because CB can induce the aggregation of P(NDI2OD-T2) molecules and prolong the film-forming time, thus leading to the change of P(NDI2OD-T2) molecular orientation. And this phenomenon also occurs in PTB7-th: P(NDI2OD-T2) blends. Due to the consistent orientation of donor and acceptor molecules, resulting in a pronounced built-in electric field that enhances exciton dissociation. The reason for this is

that CB has the ability to cause the clustering of P(NDI2OD-T2) compounds and extend the duration of film-forming, ultimately resulting in the alteration of P(NDI2OD-T2) molecular orientation. Furthermore, this occurrence is also observed in blends of PTB7-th and P(NDI2OD-T2). The optimization is credited to the aligned positioning of donor and acceptor molecules, leading to a significant pronounced electric field that boosts the dissociation of excitons.

The mixing solvent can change the crystallization sequence and optimize the phase separation structure of the blends. Zhang et al. studied the effect on microstructure by changing the order of crystallization of donor and acceptor in the P3HT:N2200 blend.[108] When N2200 had a molecular weight lower than 50.0 kDa, both polymers crystallized simultaneously in a solution of CB. However, when Ani/Tol was employed as the co-solvent, P3HT exhibited a preference for crystallization over N2200. When the average molecular weight is greater than 72.0 kDa, the crystallization of N2200 happens faster than P3HT, completing preferentially within a similar time frame. As shown in Figure 6g, they discovered that when the two components crystallize at the same time, they form larger size structures. When P3HT preferentially crystallizes, the microstructure is dominated by P3HT fiber crystals can be formed, and the molecular orientation tends to be edge-on orientation. The microstructure is mainly composed of fibrous crystals of N2200 when it crystallizes preferentially, and the molecular orientation tends to be face-on orientation, increasing the likelihood of forming the interpenetrating network structure. The findings demonstrate that the order in which crystallization occurs is a critical factor in shaping the microstructure of polymer blends.

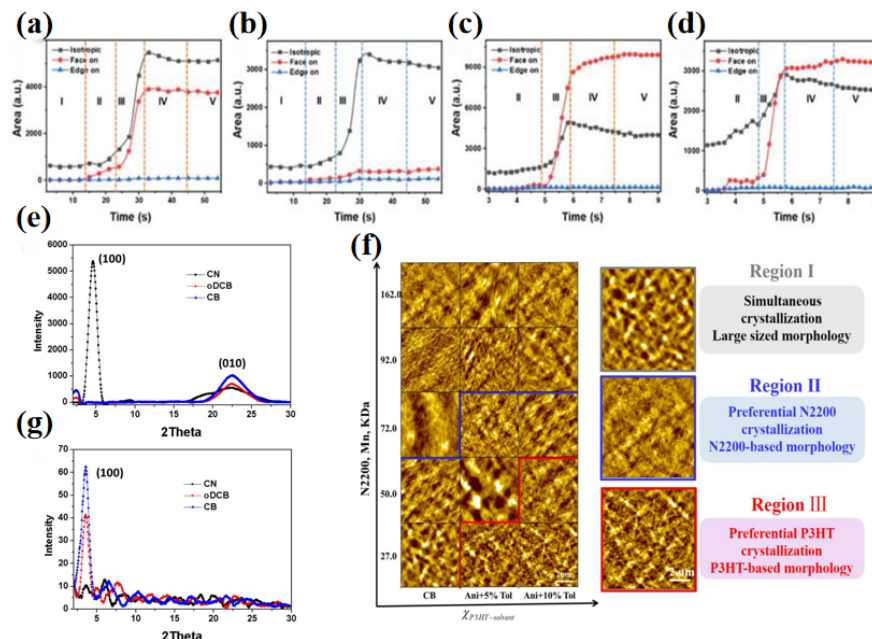


Figure 6. The change in the area of crystallite orientation (100) for (a) PDTBT2T-FTBBDT and (b) BTP-4F with CB, (c) PDTBT2T-FTBBDT and (d) BTP-4F with CF. Reproduced from [106]. (e) Out-of-plane and (f) in-plane GIXD diffraction intensity for PTB7-th:P(NDI2OD-T2) film with CN, *o*-DCB and CB. Reproduced from [107]. (g) AFM height images of P3HT:N2200 blend films. Reproduced from [108].

4.3 Adjusting the processing temperature

The effect of temperature on the morphology is mainly achieved by controlling the interaction between polymer and small molecule and the molecular diffusion rate in the active layer. The ordered aggregation or deaggregation of molecules in the solution can be promoted by adjusting the temperature of the solution. [109-111] In general, appropriately raising the temperature helps to enhance interactions, increase the rate

of molecular diffusion, and facilitate processes such as phase separation and self-assembly. All factors lead to better morphology.

The temperature has effect on the molecular solubility. Liang et al. control the nucleation rate and grain growth rate by adjusting the content of ordered aggregates in the PffBT4T-2OD:N2200 blending system.[112] At low temperature (25-65 °C), PffBT4T-2OD reaches saturated concentration, the nucleation barrier is low, and the solution contains many crystal nucleuses of PffBT4T-2OD. However, the high viscosity of the solution obstructs the molecular chain movement, resulting in low crystal growth rate, and the rate of nucleation does not match the rate of growth. The slope of the curve $K_a=0.42$ was calculated by the UV-vis absorption spectrum in situ, which can reflect the crystallization rate. When the temperature rises (65-100 °C), the molecular chain starts to move, resulting in an increase in the rate of crystallization ($K_a = 1.86$), and the nucleation and growth rate become synchronized. With a subsequent rise in temperature (100-120 °C), the elevated temperature of the solution leads to an escalation in the nucleation barrier, resulting in a rapid crystallization rate ($K_a = 19.21$) that does not align with the rate of crystal nucleation and growth. After the creation of a solution at 95 °C (Figure 7a-c), the film exhibited the highest level of crystallinity.

In addition, the temperature also affects the aggregation state of the solution. Zhou et al. studied the solution aggregation behavior at different temperatures.[113] As shown in the Figure 7d, the areas between dashed lines indicates the nano network structure can be formed at the current ratio of donor/acceptor, and the squares and circles indicate the domain size. As the temperature rises, the domain size decreases significantly. The insensitivity of *p*-DTS(FBTTh₂)₂ to temperature causes a significant portion of P(NDI2OD-T2) aggregates to transform into amorphous molecules as temperature increases. Before substantial aggregation of *p*-DTS(FBTTh₂)₂ occurring, The majority of *p*-DTS(FBTTh₂)₂ molecules are enclosed by the P(NDI2OD-T2) framework. Excitons are more likely to diffuse to the donor/acceptor interfaces. When the temperature is 80 °C, PL intensity of the film after solidification decreased by a quarter, indicating significant enhancement of exciton dissociation (Figure 7e).

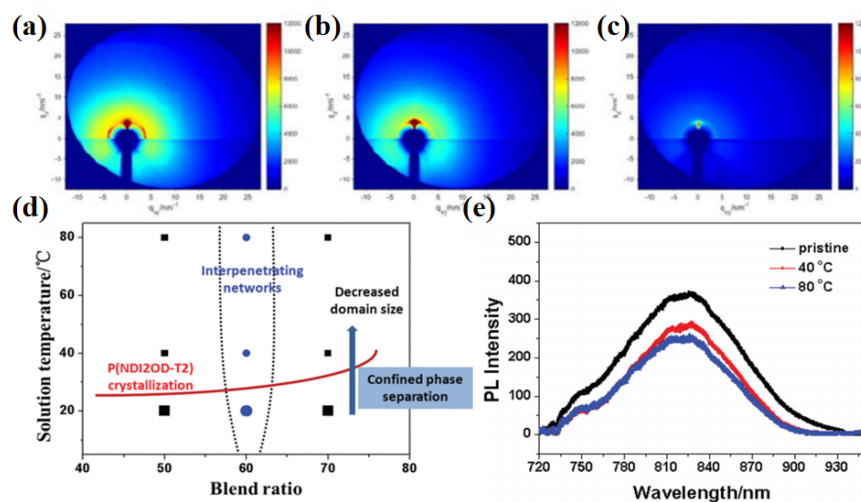


Figure 7. (a-c) The 2D GIXRD patterns for PffBT4T-2OD:N2200 blend film at 55, 95, 120 °C. Reproduced from[112]. (d) The region enclosed by dashed boundaries signifies the formation of an interpenetrating network. The beginning of P(NDI2OD-T2) crystallization is indicated by the red line, and the domain size diminishes following the phase separation that occurs within the crystallization-constrained phase. Reproduced from[113]. (e) PL profiles of blend films at different temperatures. Reproduced from[113].

4.4 Using additives

Additive treatment is an effective means to optimize the morphology. This method is to add a small amount

of additives which are quite different from the properties of the main solvent into the solution, and to control the morphology of the active layer by changing the state of the solution and film-forming kinetics.[24, 114] The introduction of additives can generally reduce solvent volatilization rate, prolong film-forming time and enhance crystallinity. At the same time, additives generally have selective solubility, which can adjust the precipitation sequence of molecules and effectively adjust the phase separation structure.[115] In addition, adding solid additives can inhibit the further phase separation and improve the stability.[116]

4.4.1 Change the film-forming time

Because the boiling point of some additives is higher than the boiling point of the solvent, the additive often remains after the solvent evaporates, continuing to induce molecular crystallization, and extending the film-forming time. Liu et al. studied how additives with different boiling points affected the film-forming process.[41] They divided the additives into two categories, high boiling point (CF) and low boiling point (DCB, TCB, CN). The crystallization behavior without and with additives is shown in Figure 8a-f. The low boiling point additive (CF) reduces film-forming time, the domain size and crystallinity. The high boiling point additives (DCB, TCB) extended the film-forming time, and the crystallization process of P3HT and O-IDTBR was separated. However, too high a boiling point, such as CN, will lead to longer film-forming time and excessive phase separation. When using cosolvents with similar properties, those with higher boiling points require a smaller optimal content to achieve the desired morphology. Therefore, the reasonable selection of additives is very important. Zhan et al. investigated the crystallization kinetics of PM6: IT-4F film following the introduction of DIO.[117] The addition of DIO significantly prolonged the film-forming time, resulting in crystallization kinetics different from that of the film without DIO (Figure 8g, h). The solubility-driven first-step crystallization has a higher nucleation rate, resulting in an increased number of sites for polymer chains to grow. The trace solvent and DIO additive are key to starting the secondary crystallization process, providing ordered and stable fluidity for the PM6 chain. Therefore, a tightly fiber network with enhanced crystallinity is formed. Simultaneously, IT-4F molecules are being placed into this fiber network. This morphology optimization improves the mobility of holes and electrons, balances the transport, and thus PCE increased from 10.11% to 12.67%. Hernandez et al. investigated the effect of additives on P(T3-TPD):PC₇₁BM mixtures.[118] According to Figure 8i and j, films made without DIO undergo a simple procedure where CF rapidly evaporates, and the film usually dries approximately 3.5 seconds after the blade passes. In contrast, films made with DIO undergo a drying process that consists of two steps, which considerably prolongs the time required for drying. The reflection spectra show two separate changes. The first change indicates the end of fast CF evaporation around 2.5 seconds after the blade passes, while the second change happens when DIO evaporation finishes, which usually takes a much longer time and is often not finished until 5500 seconds. After the evaporation of CF, a film swollen with DIO is left, in which the polymer is insoluble but the fullerene can dissolve. Throughout the following 90 minutes, despite the clear indication of DIO evaporation through changes in the reflection data, there is minimal observable change in the absorbance spectra. The results indicate that DIO has a part in increasing the density of nucleation in the early phases of film-forming, leading to a decrease in the domain size. Simultaneously, the prolonged period in which DIO forms a film encourages uninterrupted expansion of crystals, thereby enhancing the domain size. The reduced domain size led to an expansion of the surface area of the polymer fullerene, leading to a rise in FF from 44% to 61%. Consequently, the performance of OSCs was enhanced.

PM6:ITIC blend by adding DIO to it.[93] Following the introduction of DIO, a decrease in the PM6 (001) CCL from 12.5 to 2.5 nm is detected through in situ GIWAXS analysis. Additionally, there is an increase in the PM6 (100) CCL, indicating a length scale reduction in the backbone and a rearrangement of the alkyl side chains. In addition to this, in the third stage, the residual DIO continues to induce crystalline formations, filling in the fiber network. The presence of a small amount of solvent and DIO additive during the continuous crystallization process leads to the formation of lamellae-ordering length scales and a reduction in the coherence length of the polymer backbone. This causes the fragmentation of the polymer backbone into smaller fragments. The fragmentation occurs as a means to adapt to internal stress arising caused by chain ordering in other directions and the neighboring ITIC crystallites. The findings suggest that DIO has the effect of weakening the planarization of the polymer backbone while strengthening the interaction of the side chains of PM6. This causes local crystal fragmentation and the formation of fiber structures through connecting chains. At the same time, ITIC is distributed evenly across the tightly interpenetrated fiber network (Figure 9b). In the end, device PCE increased from 8.77% to 9.59%.

4.4.3 Change crystallization sequence

Some additives have different solubility for donors and acceptors, allowing them to crystallize at different stages. Liu et al. reduced the domain size to 11.2 nm by changing the crystallization sequence of the PBDB-T: PNDI blends.[120] As shown in the Figure 9c, if the donor and acceptor crystallize at the same time, it is easy to form a larger domain size due to the strong phase separation driving force (Process I). The presence of diphenyl ether (DPE) hindered the preaggregation of PBDB-T, and only the crystallization process of PNDI was observed. PBDB-T is enclosed within the PNDI structure during the SVA procedure (Process II). As a result, an ideal molecular orientation and an optimal domain size give rise to the formation of a highly crystalline interpenetrating network. The optimized structure is suitable for a range of processes, including the separation of excitons, effective movement of charges, and the prevention of charge recombination between two molecules. In the end, PCE increased from 6.55% to 7.78%. Liang et al. added TCB to P3HT:O-IDTBR to change the molecular crystallization order.[121] As shown in the Figure 9d, due to the selective dissolution and the high boiling point of TCB, P3HT crystallizes in advance and the film-forming time is prolonged. To avoid mutual interference, the crystallization procedures of P3HT and O-IDTBR are conducted separately. Furthermore, by incorporating TCB, the aggregation of P3HT takes place prior to the L-L phase separation, resulting in the formation of an interpenetrating network. By prolonging the film-forming procedure, there is sufficient time for O-IDTBR to move downwards and for P3HT to ascend, consequently improving the vertical arrangement of the film. The better morphology significantly improves charge transfer, resulting in a 7.18% increase in PCE from 4.45%. Combined with the additive and SVA, the crystallization sequence can be changed to reduce the domain size.

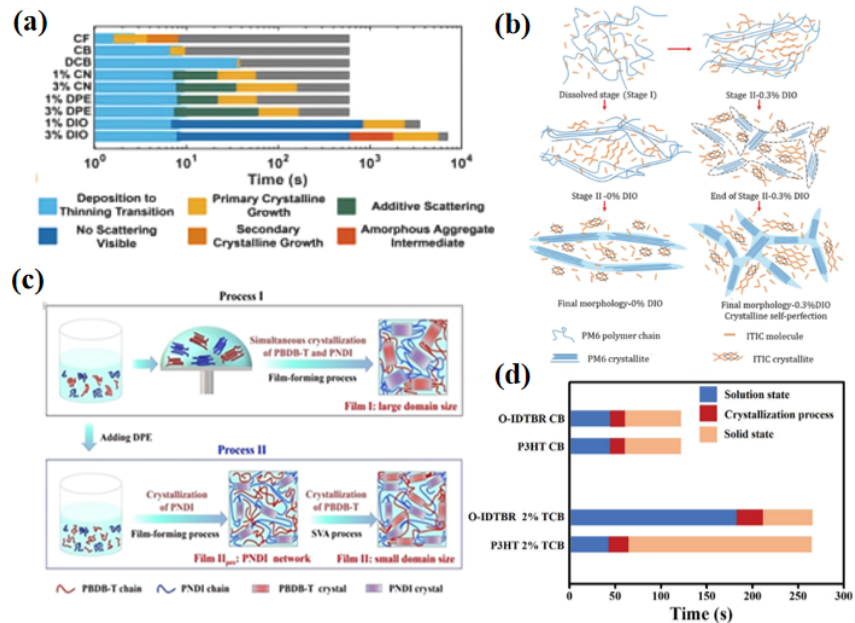


Figure 9. (a) A summary of the crystalline evolution of PTB7 is provided for the specified solvent and additive combinations. Various stages of development are marked, with the presence of gray regions indicating the absence of further progression. Reproduced from [119]. (b) The film-forming process with 0% or 0.3% DIO. Reproduced from [93]. (c) The schematic diagram of crystallization kinetics. Reproduced from [120]. (d) The abridged graph of film-forming process with and without TCB. Reproduced from [121].

4.4.4 Solid additive

Solid additives can reduce the surface energy between donor and acceptor, inhibit the increase of the active layer phase separation structure at high temperature, and achieve high stability.[116, 122-124] Fan et al. used a photoinitiator, bifunctional benzophenone, added to PBDB-T:ITIC films as a non-volatile solid additive.[125] AFM measurements show that solid additives have little effect on the surface morphology of the blend film. Nevertheless, they are effective in enhancing the π - π stacking of the polymer donor, promoting a more favorable face-on orientation (Figure 10a-i). With the addition of BP-BP, the efficiency of the PBDB-T:ITIC device increased from 10.61% to 11.89%. Yan et al. introduced volatile solid additives into J51:N2200 blend system.[126] The additive 4,40 bipyridine was dissolved in chloroform together with the active layer and was removed after hot annealing at 130 ° C for 10 minutes. Bipy can enhance the π - π packing of N2200 and increase the connectivity between the crystal layers. In the process of volatilization, the authors demonstrate that bipy interacts with N2200, resulting in the buildup of N2200 on the surface of the film. The blend experiences a more advantageous vertical phase separation as a consequence of this interaction (Figure 10j). A decrease in the number of donor/acceptor interfaces led to a small decline in J_{sc} , but a notable rise in V_{oc} and FF, indicating a distinct mechanism of action compared to other volatile solid additives.

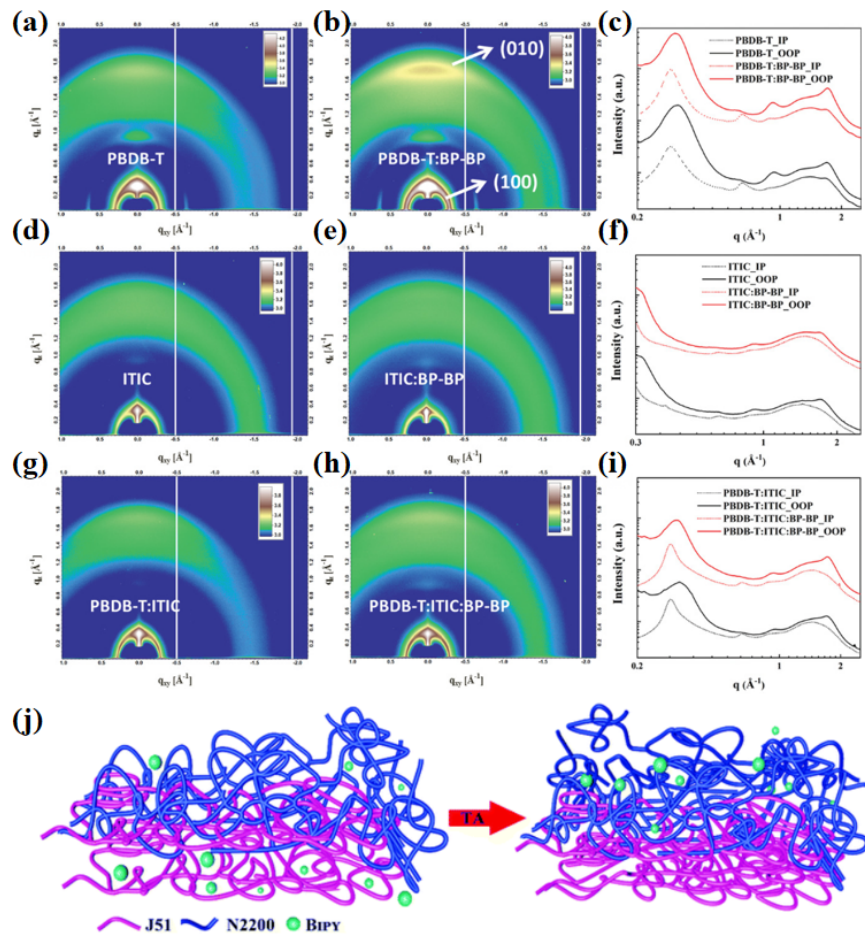


Figure 10. (a) 2D GIWAXS patterns based on (a–c) PBDB-T, (d–f) ITIC, and (g–i) PBDB-T:ITIC processed with and without BP-BP doping. Reproduced from [125]. (j) Schematic diagram of working mechanism of bipy additive before and after hot annealing in J51:N2200 blending system. Reproduced from [126].

5 Regulation of post-processing process

Post annealing treatment is a commonly used method to optimize the morphology of the active layer, which is mainly divided into TA and SVA. Their essence is to improve the movement ability of molecules, and promote its transition from metastable to stable state, so as to optimizing the device performance.

5.1 Thermal annealing

TA plays a crucial role in optimizing the morphology, and it has been demonstrated to have a positive impact on charge transport, structure development, and device performance.[127] The film is heated and evaporated for several minutes, allowing it to reshape and self-aggregate in the process.[128-130] This can enhance the crystallinity of molecules, and enhance phase purity, which leads to improved molecular orderliness and phase separation in the material.[131, 132] Since temperature can promote molecular movement, an appropriate increase in temperature during the annealing process can promote molecular movement, improve crystallization and phase separation, but too high a temperature will lead to too much phase separation.[112] In addition, the annealing time is also very important, a shorter annealing time will lead to insufficient movement of the molecules, the degree of phase separation is small, and a longer annealing time will lead to a larger phase separation.[133]

Different TA methods lead to different film-forming kinetics. Two-step TA is beneficial to improve crystallinity and phase separation. Cheng et al. used a two-step TA method to achieve DRTT-T:N3 blend films with highly ordered molecular stacking.[134] The materials are annealed at $T_{c,onset}$ of DRTT-T to induce nucleation and crystallization of the donor material. Subsequently, they undergo annealing at 130 °C for a very brief duration. This second annealing step promotes the formation of more ordered packing for both the acceptor and donor molecules simultaneously but does not lead to coarsening due to the donor nucleus being limited by diffusion. The donor nucleate in specific areas when annealing at $T_{c,onset}$, as depicted in Figure 11a. Simultaneously, the acceptor aggregate around these crystal nuclei. Following this, the process of heating above the $T_{c,onset}$ promotes the acceptor and donor molecules to adopt a more organized arrangement and attain a suitable phase segregation. Hence, the TA method with two steps can enhance device efficiency, enhance molecular arrangement, and achieve suitable phase segregation. The PCE of devices with a two-step TA process achieves 13%, surpassing the efficiency of devices annealed with a one-step process. The upside-down thermal annealing (DTA) is also an effective method to adjust the morphology. Zhang et al. propose a novel upside-down thermal annealing (DTA) method for conditioning PffBT4T-2OD:PC₇₁BM thick films.[135] After undergoing the DTA treatment, there was a noteworthy 15% enhancement in PCE, when compared to the traditional method of thermal annealing. The enhanced performance can be credited to the better organized π - π stacking of the PffffBT4T-2OD structure and the rearrangement of PC₇₁BM compounds. The AFM findings indicate that applying DTA treatment can restrict the excessive clustering of PffffBT4T-2OD on the surface, leading to an enhanced interface between the donor and acceptor (D/A) that promotes charge transportation (Figure 11b). It can also be seen from the SEM image that PffBT4T-2OD:PC₇₁BM blend film has more obvious fiber structure. This is because PffBT4T-2OD molecular packing increase after the DTA process, resulting in PC₇₁BM molecular redistribution. This phenomenon plays a role in establishing continuous pathways for carrier transport within the mixed region, leading to the enhancement of phase separation in thick films. The likelihood of excitons reaching the D/A interface is enhanced by these findings, which aids in charge transport and electron collection, ultimately resulting in higher J_{sc} and FF.

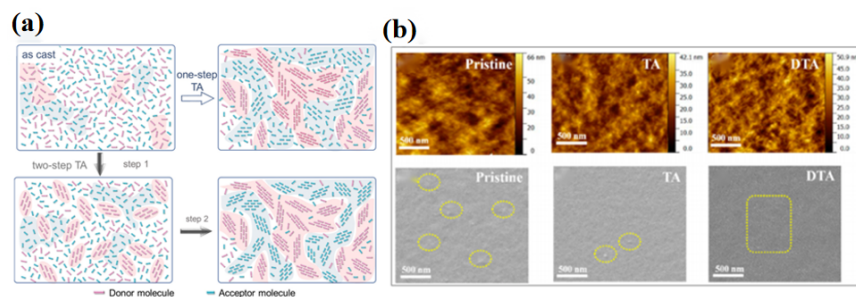


Figure 11. (a) This diagram illustrates the changes in the structure of DRTT-T:N3 blend films when subjected to one-step and two-step TA. Reproduced from [134]. (b) AFM and TEM pictures with pristine, TA, and DTA. Reproduced from [135].

In the TA process, the control of parameters is also very important. Levitsky et al. studied the effect of different annealing temperatures on the film-forming process.[136] PCE11:PCBM blend films were annealed at different times at 80, 110, 125 and 140. Subsequently, these films were regularly examined using optical microscopy (Figure 12a). Higher temperatures facilitate the dispersion of PCBM molecules, leading to accelerated aggregate growth, ultimately leading to decreased density and increased aggregate size. The temperature of 150 is in closer proximity to the metastable monotectic temperature, consequently resulting in a reduced driving force for PCBM nucleation in comparison to 130. Due to the inverse relationship between the nucleation barrier and the square of the driving force, the barrier at 150 is significantly greater compared to 130. As a result, the rate of nucleation at a temperature of 150 is significantly less than that at 130. The findings indicate that following annealing at a temperature of 150, the film exhibits a reduced

presence of sizable PCBM particles, with the presence of unaltered spinodal microstructure interspersed throughout. As a result, after annealing at 150 °C, substantial crystalline PCBM aggregates have already formed, while a bicontinuous spinodal-like phase separation persists due to the slow nucleation rate of crystalline PCBM. The rate of molecular diffusion can be influenced by temperature. Liang et al. changed the TA temperature to investigate the effect of the molecular diffusion rate on *p*-DTS(FBTTh₂)₂:EP-PDI blend films.[112] As shown in Figure 12b, when the annealing temperature is lower than 90 °C, EP-PDI and *p*-DTS(FBTTh₂)₂ are almost uniformly mixed, and there is no obvious phase separation structure. When the temperature is between 90 °C and 130 °C, the film forms a nanoscale interpenetrating network structure, which not only facilitates exciton separation, but also ensures efficient carrier transport. When the annealing temperature was higher than 130 °C, the crystallinity of EP-PDI increased significantly, which dominated the film morphology and formed large phase separation. Figure 12c shows the fluorescence spectra. The molecular diffusion rate of the blend system can be divided into the following three stages, as shown in Figure 12d, When the temperature is lower than 90 °C (blue area), the molecular diffusion rate of both films is relatively slow, and the films have no obvious phase separation structure. When the temperature is between 90 °C and 130 °C (purple region), the diffusion rate of EP-PDI molecules is faster than that of *p*-DTS(FBTTh₂)₂ molecules, and *p*-DTS(FBTTh₂)₂ crystals form a network skeleton structure, which restricts the diffusion of EP-PDI molecules. During the cooling process, EP-PDI formed microcrystals and filled in the *p*-DTS(FBTTh₂)₂ crystal frame, forming nanoscale interpenetrating network structure. When the temperature exceeds 130 °C (yellow region), the molecular diffusion rate of both films is faster, and EP-PDI breaks through the restriction, and the film phase separation size further increases. Therefore, reasonable control of molecular diffusion rate is an effective way to construct the interpenetrating network structure of active layer.

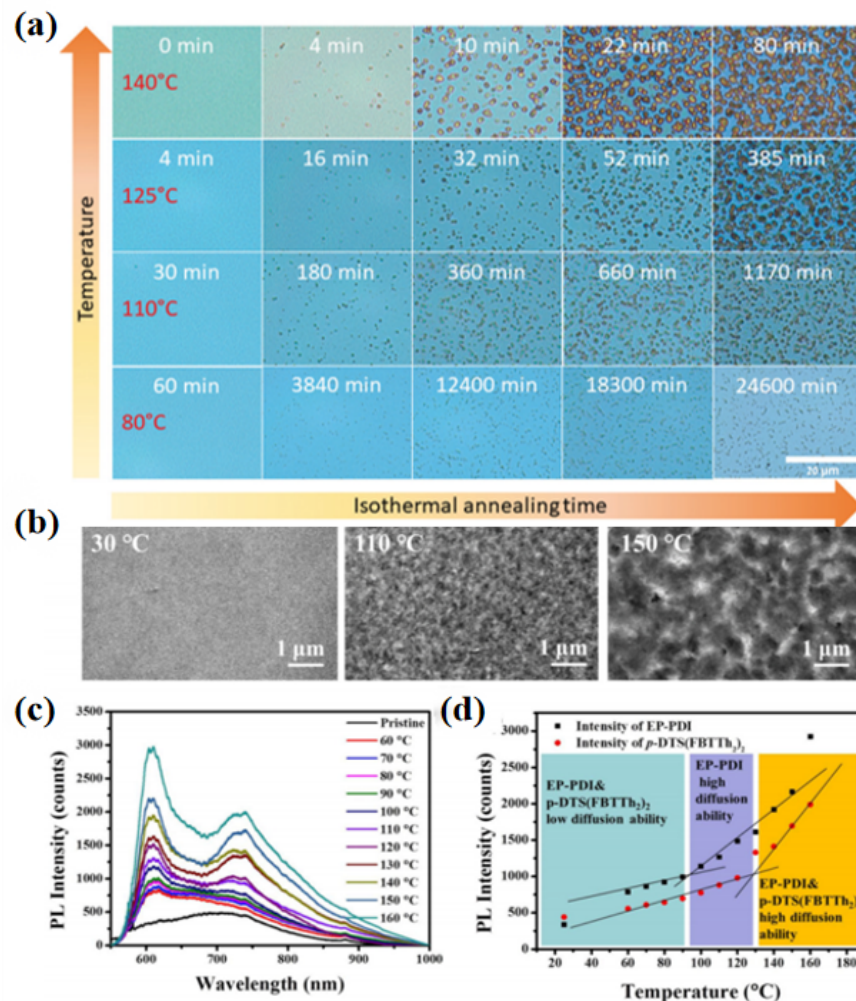


Figure 12. (a) Optical micrographs of PCE11:PCBM films captured during various isothermal annealing steps at temperatures of 140, 125, 110, and 80 °C. Reproduced from [136]. TEM images (b) and fluorescence spectra (c) of the blend film were processed at different temperatures. Reproduced from [112]. (d) Changes in the fluorescence intensity of blend films at 620 and 725 nm when subjected to various temperatures. Reproduced from [112].

5.2 Solvent vapor annealing

Another approach to control the morphology is SVA. Following the casting process, the film is promptly transferred to a chamber containing a greater concentration of solvent in SVA. Throughout this procedure, the solvent vapor infiltrates the film, influencing its structure. The vapor of the solvent has the ability to enhance the movement of molecules, providing them with additional time to rearrange and enhancing the quality of the film's structure.[137] One benefit of SVA is its ability to be carried out at lower temperatures. Research has shown that it is effective even without an inert atmosphere, thereby verifying the possibility of its execution and enhancement.[138] The impact of a specific solvent on the active substance relies on various elements, encompassing its ability to dissolve, polarity, and experimental factors. The aggregation of PCBM and the crystallization of the polymer can be influenced by the use of highly volatile annealing solvents in polymer-fullerene systems.[69, 139]

The choice of solvent is the most important part of solvent annealing. Different solvents will affect the

optimum annealing time. Christina et al. found that the optimal annealing time was inversely related to the donor solubility.[140] They used four solvents (CHCl_3 , THF, CS_2 , and $\text{C}_3\text{H}_6\text{O}_2$), each showing a different solubility to the donor. By analyzing Figure 13a, the entire SVA process can be divided into three stages. During the initial stage, the solvent infiltrates the film and causes additional phase separation in the finely grained structures present in the as-cast state. During the second stage, these structures begin to grow. Because this growth is facilitated by diffusion mechanisms, diverse nanomorphologies develop under different solvent vapor atmospheres. Therefore, the rate of the diffusion is directly proportional to the solubility of the solvent being used. Following this linear growth regime, the DRCN5T fibers enter the subsequent sublinear growth phase characterized by the maturation and saturation of the structures in the final phase. In summary, if the solubility of the donor is low, the growth of the fiber will be slower and the annealing time will be longer. Appropriate solvents help to reduce domain size. Engmann et al. improved the phase size by adding THF to BTR:PC₇₁BM blends.[32] During the initial phases of the SVA, when the film is exposed to CF, it leads to the dissolution of small imperfect crystals. The enhancement in film crystallization and phase purity is not apparent until the CF concentration in the vapor of the annealing chamber is decreased. The dissolution at the beginning leads to a decrease in nucleation density, resulting in the growth of a small number of crystals to a larger size, approximately 60 nm in domain size. When using a moderate solvent such as THF, the ability to dissolve tiny crystals decreases, leading to a comparatively higher density of nucleation. Nevertheless, the size of the crystals in general stays small, and the occurrence of excessive film coarsening is avoided. In all instances, an elevation in scattering intensity is noted during the annealing process, which signifies an enhancement in phase purity. This increase is accompanied by a noticeable expansion of characteristic length scales, indicating the coarsening of domains (Figure 13b). After the addition of THF, the phase region size is the smallest, about 30 nm. Han et al. induced phase separation of PC₇₁BM and PCDTBT side chains by mixing solvents.[141] THF can effectively promote the crystallization of fullerene molecules, while CS_2 can effectively increase the molecular motivity and promote the aggregation of polymer molecules. As shown in Figure 13c, On the basis of increasing molecular migration and diffusion ability, mixed steam treatment can promote the aggregation of fullerene molecules and induce phase separation between polymer side chain and fullerene. Fullerene aggregates react with polymers, reducing the degree of entanglement between polymers. Finally, the self-organizing ability of the polymer is improved, the crystal size is increased, and the interpenetrating network structure is formed.

Selecting the appropriate annealing method is also an effective strategy to optimize the morphology. The combination of TA and SVA can change the molecular crystallization sequence. Liang et al. prepared a highly crystalline network by adjusting the sequence of TA and SVA.[142] Films I and II showed more pronounced absorption near 635 nm compared to the original films, indicating increased crystallinity of PBDB-T. However, only Film I exhibits a noticeable rise in absorption at 700 nm, suggesting that the crystallinity of ITIC may have been improved during the TSA-I process (Figure 13d). The results of crystallization kinetics show that the crystallization of ITIC is significantly enhanced when the crystallization of ITIC occurs before the establishment of the PBDB-T crystal network. This is primarily because the diffusion of ITIC molecules is less constrained under these conditions. However, if PBDB-T crystallize preferentially, the fusion of ITIC is limited by the PBDB-T crystal network, leading to a lower crystallinity of ITIC. The results show that the performance of the device is improved from 8.02% to 10.95%. Xie et al. also used the combined method of SVA and TA to treat P3HT:PCBM films.[143] They treated the film with DCB as solvent vapor. The absorption spectra show that the absorption spectra of P3HT have a redshift, an increase in intensity, and a new peak in long wave strength (Figure 13e). This shows that the length of the P3HT conjugated chains increases and that an ordered structure is formed between the chains. PCBM aggregates appeared in large quantities and formed phase separation structure after annealing at 150 °C.

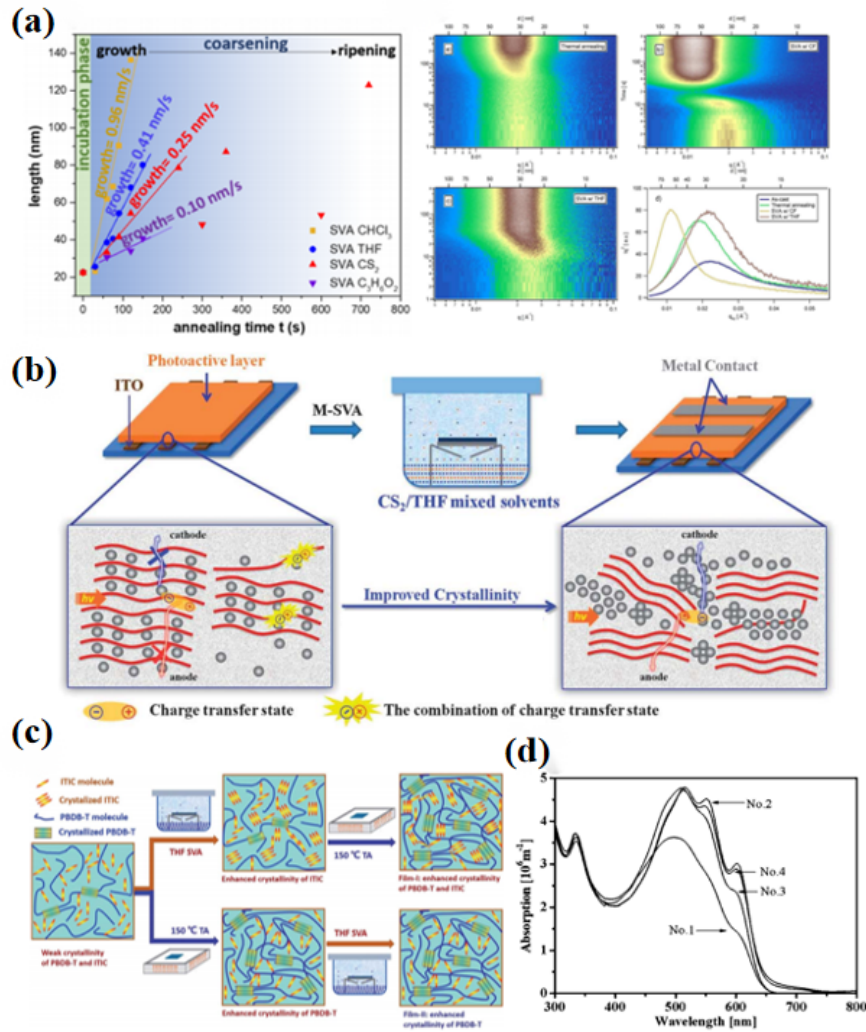


Figure 13. (a) Change of the growth rate of DRCN5T fibers with annealing time (CHCl_3 , THF, CS_2 , and $\text{C}_3\text{H}_6\text{O}_2$). Reproduced from [140]. (b) Evolution of the q_2 -weighted background corrected GISAXS intensity near the sample horizon ($q_z \approx 0$). And the background corrected scattering intensity. Reproduced from [32]. (c) Schematic illustration of the morphology transition. Reproduced from [141]. (d) Crystallization of PBDB-T in different TA and SVA processing sequences. Reproduced from [142]. (e) UV-vis absorption spectra, including pristine (No. 1), DCB vapor treated (No. 2), annealed (No. 3), and DCB vapor treated and annealed (No. 4). Reproduced from [143].

6 Conclusion

In conclusion, we elaborated the characterization method and regulation strategy for regulating the crystallization kinetics and revealed the underlying mechanism. First, we introduce the characterization methods, including UV-vis absorption spectroscopy, PL, GIWAXS and GISAXS. Subsequently, we introduced the regulation method of film-forming process and post-annealing process and the mechanism of influence on morphology, including film-forming method, solvent, temperature, additive, TA and SVA. Through this review, we hope to deepen our understanding of the effects of crystallization dynamics on the morphology, which may guide to achieve higher device performance.

Since the appearance of OSCs, they have attracted extensive attention. In order to promote the industrialization of OSCs, efforts can be made from the following aspects: (1) Better materials, including electrode materials, active layer materials and interface layer materials, especially environmentally friendly materials should be designed; (2) A deeper understanding of the relationship between fabricating conditions-morphology-device performance; (3) development of the characterization methods; (4) Meet the requirements of practical applications such as stability and large-area solution fabrication of devices.

Acknowledgements

This work was supported by the National Natural Science Foundation of China (52073231, 62304181), the Shaanxi Provincial High level Talent Introduction Project (5113220044), the Shaanxi Outstanding Youth Project (2023-JC-JQ-33), the Youth Science and Technology Talent Promotion Project of Jiangsu Association for Science and Technology (TJ-2022-088), the Project funded by China Postdoctoral Science Foundation (2023TQ0273, 2023TQ0274), the Natural Science Basic Research Program of Shaanxi (2023-JC-QN-0726), Guangdong Basic and Applied Basic Research Foundation (2022A1515110286), the National Aerospace Science Foundation of China (2020Z073053010), the Suzhou Science and Technology Development Plan Innovation Leading Talent Project (ZXL2023183), the Fundamental Research Funds for the Central Universities (G2022KY05108, G2023KY0605, G2023KY0601), the NWPU research fund for young scholars (G2022WD01014), the Natural Science Foundation of Chongqing, China (cstc2021jcyj-msxmX0990), the Basic Research Programs of Taicang, 2021 (TC2021JC08).

References

- [1] B. Liu, Y. Xu, D. Xia, C. Xiao, Z. Yang, W. Li, Semitransparent Organic Solar Cells based on Non-Fullerene Electron Acceptors, *Acta Phys.-Chim. Sin.* 37(3) (2020) 2009056-0.
- [2] L. Zhan, S. Yin, Y. Li, S. Li, T. Chen, R. Sun, J. Min, G. Zhou, H. Zhu, Y. Chen, J. Fang, C.Q. Ma, X. Xia, X. Lu, H. Qiu, W. Fu, H. Chen, Multiphase Morphology with Enhanced Carrier Lifetime via Quaternary Strategy Enables High-Efficiency, Thick-Film, and Large-Area Organic Photovoltaics, *Adv. Mater.* 34(45) (2022) e2206269.
- [3] Z. Genene, W. Mammo, E.G. Wang, M.R. Andersson, Recent Advances in n-Type Polymers for All-Polymer Solar Cells, *Adv. Mater.* 31(22) (2019) 40.
- [4] C. Lee, S. Lee, G.U. Kim, W. Lee, B.J. Kim, Recent Advances, Design Guidelines, and Prospects of All-Polymer Solar Cells, *Chem. Rev.* 119(13) (2019) 8028-8086.
- [5] H.F. Yao, J.W. Wang, Y. Xu, S.Q. Zhang, J.H. Hou, Recent Progress in Chlorinated Organic Photovoltaic Materials, *Acc. Chem. Res.* 53(4) (2020) 822-832.
- [6] P. Cheng, G. Li, X. Zhan, Y. Yang, Next-generation organic photovoltaics based on non-fullerene acceptors, *Nat. Photonics* 12(3) (2018) 131-142.
- [7] Y.F. Li, All-Small-Molecule Organic Solar Cells: Hierarchical Morphology Control Achieves Efficiency Breakthrough, *Acta Phys Chim Sin* 36(7) (2020) 2.
- [8] X.Y. Xu, H.B. Wu, S.J. Liang, Z. Tang, M.Y. Li, J. Wang, X. Wang, J. Wen, E.J. Zhou, W.W. Li, Z.F. Ma, Quantum Efficiency and Voltage Losses in P3HT:Non-fullerene Solar Cells, *Acta Phys Chim Sin* 38(11) (2022) 11.
- [9] X.J. He, C.C.S. Chan, X.H. Zou, S. Zhang, P.W.K. Fong, J. Kim, G. Li, X.T. Hu, W. Ma, K.S. Wong, W.C.H. Choy, Modulating the Mixing Gibbs Free Energy to Enhance Solid-Liquid Phase Separation for High-Performance Organic Solar Cells, *Adv. Mater.* 13(11) (2023) 10.
- [10] J.Q. Wang, Z. Zheng, P.Q. Bi, Z.H. Chen, Y.F. Wang, X.Y. Liu, S.Q. Zhang, X.T. Hao, M.J. Zhang, Y.F. Li, J.H. Hou, Tandem organic solar cells with 20.6% efficiency enabled by reduced voltage losses, *Natl. Sci. Rev.* 10(6) (2023) 11.

- [11] Z. He, C. Zhong, X. Huang, W.Y. Wong, H. Wu, L. Chen, S. Su, Y. Cao, Simultaneous enhancement of open-circuit voltage, short-circuit current density, and fill factor in polymer solar cells, *Adv. Mater.* 23(40) (2011) 4636-43.
- [12] Y. Chen, X. Wan, G. Long, High performance photovoltaic applications using solution-processed small molecules, *Acc. Chem. Res.* 46(11) (2013) 2645-55.
- [13] Y. Liu, B. Liu, C.-Q. Ma, F. Huang, G. Feng, H. Chen, J. Hou, L. Yan, Q. Wei, Q. Luo, Q. Bao, W. Ma, W. Liu, W. Li, X. Wan, X. Hu, Y. Han, Y. Li, Y. Zhou, Y. Zou, Y. Chen, Y. Liu, L. Meng, Y. Li, Y. Chen, Z. Tang, Z. Hu, Z.-G. Zhang, Z. Bo, Recent progress in organic solar cells (Part II device engineering), *Sci China Chem* 65(8) (2022) 1457-1497.
- [14] F. Qiao, K. Sun, H. Chu, J. Wang, Y. Xie, L. Chen, T. Yan, Design strategies of ZnO heterojunction arrays towards effective photovoltaic applications, *Battery Energy* 1(1) (2022).
- [15] W.B. Tarique, A. Uddin, A review of progress and challenges in the research developments on organic solar cells, *Mater. Sci. Semicond. Process* 163 (2023) 22.
- [16] L.C. Sun, Y.C. Chen, M.T. Sun, Y.J. Zheng, Organic Solar Cells: Physical Principle and Recent Advances, *Chem.-Asian J.* (2023) 13.
- [17] H.K. Kim, H. Yu, M. Pan, X. Shi, H. Zhao, Z. Qi, W. Liu, W. Ma, H. Yan, S. Chen, Linker Unit Modulation of Polymer Acceptors Enables Highly Efficient Air-Processed All-Polymer Solar Cells, *Adv Sci* 9(25) (2022) e2202223.
- [18] L. Zhan, S. Li, Y. Li, R. Sun, J. Min, Z. Bi, W. Ma, Z. Chen, G. Zhou, H. Zhu, M. Shi, L. Zuo, H. Chen, Desired open-circuit voltage increase enables efficiencies approaching 19% in symmetric-asymmetric molecule ternary organic photovoltaics, *Joule* 6(3) (2022) 662-675.
- [19] Z. Bi, H.B. Naveed, H. Wu, C. Zhang, X. Zhou, J. Wang, M. Wang, X. Wu, Q. Zhu, K. Zhou, K. Chen, C. Wang, Z. Tang, W. Ma, Tuning Acceptor Composition in Ternary Organic Photovoltaics-Impact of Domain Purity on Non-Radiative Voltage Losses, *Adv. Mater.* 12(18) (2022).
- [20] P. Koli, R. Kumar, Y. Dayma, R.K. Pareek, A. Meena, M. Jonwal, Tropaeoline O-oxalic acid-benzalkonium chloride photogalvanic cells for solar energy conversion and storage, *Battery Energy* 1(4) (2022).
- [21] X.Y. Mu, Y.W. Ji, H. Yin, K. Gao, Interfacial Hole-Charge-Transfer Dynamics in Organic Solar Cells: A Dynamic, *Phys. Rev. Appl.* 19(5) (2023) 10.
- [22] B.W. Sun, N. Tokmoldin, O. Alqahtani, A. Patterson, C.S.P. De Castro, D.B. Riley, M. Pranav, A. Armin, F. Laquai, B.A. Collins, D. Neher, S. Shoaee, Toward More Efficient Organic Solar Cells: A Detailed Study of Loss Pathway and Its Impact on Overall Device Performance in Low-Offset Organic Solar Cells, *Adv. Energy Mater.* 13(26) (2023) 11.
- [23] Y.Y. Zhou, L.H. Hu, X.D. Tang, Z.T. Wang, L.L. Jiang, M. Li, R.P. Qin, Employing fullerene acceptor as the third component to enhance charge transfer for high-efficiency ternary organic solar cells, *Mater. Lett.* 341 (2023) 4.
- [24] C. McDowell, M. Abdelsamie, M.F. Toney, G.C. Bazan, Solvent Additives: Key Morphology-Directing Agents for Solution-Processed Organic Solar Cells, *Adv. Mater.* 30(33) (2018) 30.
- [25] Y. Huang, E.J. Kramer, A.J. Heeger, G.C. Bazan, Bulk Heterojunction Solar Cells: Morphology and Performance Relationships, *Chem. Rev.* 114(14) (2014) 7006-7043.
- [26] Y.C. Mao, W. Li, M.X. Chen, X.L. Chen, R.S. Gurney, D. Liu, T. Wang, Evolution of molecular aggregation in bar-coated non-fullerene organic solar cells, *Mat. Chem. Front.* 3(6) (2019) 1062-1070.

- [27] J. Liu, L. Chen, B. Gao, X. Cao, Y. Han, Z. Xie, L. Wang, Constructing the nanointerpenetrating structure of PCDTBT:PC₇₀BM bulk heterojunction solar cells induced by aggregation of PC₇₀BM via mixed-solvent vapor annealing, *J. Mater. Chem. A* 1(20) (2013).
- [28] D. Yang, S. Grott, X.Y. Jiang, K.S. Wienhold, M. Schwartzkopf, S.V. Roth, P. Muller-Buschbaum, In Situ Studies of Solvent Additive Effects on the Morphology Development during Printing of Bulk Heterojunction Films for Organic Solar Cells, *Small Methods* 4(9) (2020) 7.
- [29] C.L. Radford, R.D. Pettipas, T.L. Kelly, Watching Paint Dry: Operando Solvent Vapor Annealing of Organic Solar Cells, *J. Phys. Chem. Lett.* 11(15) (2020) 6450-6455.
- [30] J. Xin, W. Li, Y. Zhang, Q. Liang, C. Song, Y. Zhao, Z. He, J. Liu, W. Ma, A review of nonfullerene solar cells: Insight into the correlation among molecular structure, morphology, and device performance, *Battery Energy* 2(2) (2022).
- [31] B. Schmidt-Hansberg, M. Sanyal, M.F.G. Klein, M. Pfaff, N. Schnabel, S. Jaiser, A. Vorobiev, E. Muller, A. Colsmann, P. Scharfer, D. Gerthsen, U. Lemmer, E. Barrena, W. Schabel, Moving through the Phase Diagram: Morphology Formation in Solution Cast Polymer-Fullerene Blend Films for Organic Solar Cells, *ACS Nano* 5(11) (2011) 8579-8590.
- [32] S. Engmann, H.W. Ro, A. Herzing, C.R. Snyder, L.J. Richter, P.B. Geraghty, D.J. Jones, Film morphology evolution during solvent vapor annealing of highly efficient small molecule donor/acceptor blends, *J. Mater. Chem. A* 4(40) (2016) 15511-15521.
- [33] C. Lee, Y. Li, W. Lee, Y. Lee, J. Choi, T. Kim, C. Wang, E.D. Gomez, H.Y. Woo, B.J. Kim, Correlation between Phase-Separated Domain Sizes of Active Layer and Photovoltaic Performances in All-Polymer Solar Cells, *Macromolecules* 49(14) (2016) 5051-5058.
- [34] L. Ye, Y. Xiong, S.S. Li, M. Ghasemi, N. Balar, J. Turner, A. Gadisa, J.H. Hou, B.T. O'Connor, H. Ade, Precise Manipulation of Multilength Scale Morphology and Its Influence on Eco-Friendly Printed All-Polymer Solar Cells, *Adv. Funct. Mater.* 27(33) (2017) 10.
- [35] J. Manigrasso, I. Chillon, V. Genna, P. Vidossich, S. Somarowthu, A.M. Pyle, M. De Vivo, M. Marcia, Author Correction: Visualizing group II intron dynamics between the first and second steps of splicing, *Nat Commun* 13(1) (2022) 1.
- [36] Q. Yu, J. Xu, J. Fu, T. Xu, X. Yan, S. Chen, H. Chen, K. Sun, Z. Kan, S. Lu, Z. Xiao, Crystallinity dictates the selection of fullerene or non-fullerene acceptors in a small molecule organic solar cell, *Dyes Pigm.* 187 (2021).
- [37] C.Y. Yang, R.N. Yu, C.Y. Liu, H. Li, S.Q. Zhang, J.H. Hou, Achieving over 10 % Efficiency in Poly(3-hexylthiophene)-based Organic Solar Cells via Solid Additives, *ChemSusChem* 14(17) (2021) 3607-3613.
- [38] F. Liu, J.Y. Zhang, Z.C. Zhou, J.Q. Zhang, Z.X. Wei, X.Z. Zhu, Poly(3-hexylthiophene)-based non-fullerene solar cells achieve high photovoltaic performance with small energy loss, *J. Mater. Chem. A* 5(32) (2017) 16573-16579.
- [39] S.X. Li, W.Q. Liu, M.M. Shi, J.Q. Mai, T.K. Lau, J.H. Wan, X.H. Lu, C.Z. Li, H.Z. Chen, A spirofluorene and diketopyrrolopyrrole moieties based non-fullerene acceptor for efficient and thermally stable polymer solar cells with high open-circuit voltage, *Energy Environ. Sci.* 9(2) (2016) 604-610.
- [40] S. Holliday, R.S. Ashraf, A. Wadsworth, D. Baran, S.A. Yousaf, C.B. Nielsen, C.H. Tan, S.D. Dimitrov, Z.R. Shang, N. Gasparini, M. Alamoudi, F. Laquai, C.J. Brabec, A. Salleo, J.R. Durrant, I. McCulloch, High-efficiency and air-stable P3HT-based polymer solar cells with a new non-fullerene acceptor, *Nat. Commun.* 7 (2016) 11.
- [41] J.G. Liu, S.Y. Zeng, P. Jing, K. Zhao, Q.J. Liang, Investigating the effect of cosolvents on P3HT/O-IDTBR film-forming kinetics and film morphology, *J. Energy Chem.* 51 (2020) 333-341.

- [42] I. Pelse, J.L. Hernandez, S. Engmann, A.A. Herzing, L.J. Richter, J.R. Reynolds, Cosolvent Effects When Blade-Coating a Low-Solubility Conjugated Polymer for Bulk Heterojunction Organic Photovoltaics, *ACS Appl. Mater. Interfaces* 12(24) (2020) 27416-27424.
- [43] Y. Xu, H. Yao, L. Ma, L. Hong, J. Li, Q. Liao, Y. Zu, J. Wang, M. Gao, L. Ye, J. Hou, Tuning the Hybridization of Local Exciton and Charge-Transfer States in Highly Efficient Organic Photovoltaic Cells, *Angew. Chem. Int. Ed.* 59(23) (2020) 9004-9010.
- [44] L. Zhu, M. Zhang, G. Zhou, T. Hao, J. Xu, J. Wang, C. Qiu, N. Prine, J. Ali, W. Feng, X. Gu, Z. Ma, Z. Tang, H. Zhu, L. Ying, Y. Zhang, F. Liu, Efficient Organic Solar Cell with 16.88% Efficiency Enabled by Refined Acceptor Crystallization and Morphology with Improved Charge Transfer and Transport Properties, *Adv. Energy Mater.* 10(18) (2020).
- [45] H. Yao, D. Qian, H. Zhang, Y. Qin, B. Xu, Y. Cui, R. Yu, F. Gao, J. Hou, Critical Role of Molecular Electrostatic Potential on Charge Generation in Organic Solar Cells, *Chinese J. Chem.* 36(6) (2018) 491-494.
- [46] A. Ojala, A. Petersen, A. Fuchs, R. Lovrincic, C. Polking, J. Trollmann, J. Hwang, C. Lennartz, H. Reichelt, H.W. Hoffken, A. Pucci, P. Erk, T. Kirchartz, F. Wurthner, Merocyanine/C60 Planar Heterojunction Solar Cells: Effect of Dye Orientation on Exciton Dissociation and Solar Cell Performance, *Adv. Funct. Mater.* 22(1) (2012) 86-96.
- [47] M. Schubert, B.A. Collins, H. Mangold, I.A. Howard, W. Schindler, K. Vandewal, S. Roland, J. Behrends, F. Kraffert, R. Steyrleuthner, Z.H. Chen, K. Fostiropoulos, R. Bittl, A. Salleo, A. Facchetti, F. Laquai, H.W. Ade, D. Neher, Correlated Donor/Acceptor Crystal Orientation Controls Photocurrent Generation in All-Polymer Solar Cells, *Adv. Funct. Mater.* 24(26) (2014) 4068-4081.
- [48] V. Vohra, K. Kawashima, T. Kakara, T. Koganezawa, I. Osaka, K. Takimiya, H. Murata, Efficient inverted polymer solar cells employing favourable molecular orientation, *Nat. Photonics* 9(6) (2015) 403-+.
- [49] J. Jung, W. Lee, C. Lee, H. Ahn, B.J. Kim, Controlling Molecular Orientation of Naphthalenediimide-Based Polymer Acceptors for High Performance All-Polymer Solar Cells, *Adv. Energy Mater.* 6(15) (2016) 10.
- [50] J.W. Jo, J.W. Jung, H. Ahn, M.J. Ko, A.K.Y. Jen, H.J. Son, Effect of Molecular Orientation of Donor Polymers on Charge Generation and Photovoltaic Properties in Bulk Heterojunction All-Polymer Solar Cells, *Adv. Energy Mater.* 7(1) (2017) 9.
- [51] N.A. Ran, S. Roland, J.A. Love, V. Savikhin, C.J. Takacs, Y.T. Fu, H. Li, V. Coropceanu, X.F. Liu, J.L. Bredas, G.C. Bazan, M.F. Toney, D. Neher, T.Q. Nguyen, Impact of interfacial molecular orientation on radiative recombination and charge generation efficiency, *Nat. Commun.* 8 (2017) 9.
- [52] K. Nakano, K. Tajima, Organic Planar Heterojunctions: From Models for Interfaces in Bulk Heterojunctions to High-Performance Solar Cells, *Adv. Mater.* 29(25) (2017) 33.
- [53] J. Liu, H. Lu, Y. Yin, K. Wang, P. Wei, C. Song, Z. Miao, Q. Liang, Thermodynamic and kinetic insights for regulating molecular orientation in nonfullerene all-small-molecule solar cells, *Battery Energy* 1(3) (2022).
- [54] G. Yu, J. Gao, J.C. Hummelen, F. Wudl, A.J. Heeger, POLYMER PHOTOVOLTAIC CELLS - ENHANCED EFFICIENCIES VIA A NETWORK OF INTERNAL DONOR-ACCEPTOR HETEROJUNCTIONS, *Science* 270(5243) (1995) 1789-1791.
- [55] Q. Liang, Z. Hu, J. Yao, Z. Wu, Z. Ding, K. Zhao, X. Jiao, J. Liu, W. Huang, Blending Donors with Different Molecular Weights: An Efficient Strategy to Resolve the Conflict between Coherence Length and Intermixed Phase in Polymer/Nonfullerene Solar Cells, *Small* 18(3) (2022) e2103804.
- [56] J.J. Dittmer, E. And, R.H. Friend, Electron Trapping in Dye/Polymer Blend Photovoltaic Cells, *Advanced Materials* 12(17) (2000) 1270-1274.

- [57] Osterbacka, An, Jiang, Vardeny, Two-dimensional electronic excitations in self-assembled conjugated polymer nanocrystals, *Science* 287(5454) (2000) 839-42.
- [58] X.N. Yang, J. Loos, S.C. Veenstra, W.J.H. Verhees, M.M. Wienk, J.M. Kroon, M.A.J. Michels, R.A.J. Janssen, Nanoscale morphology of high-performance polymer solar cells, *Nano Lett.* 5(4) (2005) 579-583.
- [59] Y. Zhao, Z.Y. Xie, Y. Qu, Y.H. Geng, L.X. Wang, Solvent-vapor treatment induced performance enhancement of poly(3-hexylthiophene): methanofullerene bulk-heterojunction photovoltaic cells, *Appl. Phys. Lett.* 90(4) (2007) 3.
- [60] J.H. Park, J.S. Kim, J.H. Lee, W.H. Lee, K. Cho, Effect of Annealing Solvent Solubility on the Performance of Poly(3-hexylthiophene)/Methanofullerene Solar Cells, *J. Phys. Chem. C* 113(40) (2009) 17579-17584.
- [61] V. Shrotriya, Y. Yao, G. Li, Y. Yang, Effect of self-organization in polymer/fullerene bulk heterojunctions on solar cell performance, *Appl. Phys. Lett.* 89(6) (2006) 3.
- [62] B.Y. Shao, D.A.V. Bout, Probing the molecular weight dependent intramolecular interactions in single molecules of PCDTBT, *J. Mater. Chem. C* 5(37) (2017) 9786-9791.
- [63] R. Noriega, Efficient Charge Transport in Disordered Conjugated Polymer Microstructures, *Macromol. Rapid Commun.* 39(14) (2018) 9.
- [64] R. Steyrlleuthner, M. Schubert, I. Howard, B. Klaumunzer, K. Schilling, Z.H. Chen, P. Saalfrank, F. Laquai, A. Facchetti, D. Neher, Aggregation in a High-Mobility n-Type Low-Bandgap Copolymer with Implications on Semicrystalline Morphology, *J. Am. Chem. Soc.* 134(44) (2012) 18303-18317.
- [65] L.J. Richter, D.M. DeLongchamp, A. Amassian, Morphology Development in Solution-Processed Functional Organic Blend Films: An In Situ Viewpoint, *Chem. Rev.* 117(9) (2017) 6332-6366.
- [66] E. Giussani, L. Brambilla, D. Fazzi, M. Sommer, N. Kayunkid, M. Brinkmann, C. Castiglioni, Structural Characterization of Highly Oriented Naphthalene-Diimide-Bithiophene Copolymer Films via Vibrational Spectroscopy, *J. Phys. Chem. B* 119(5) (2015) 2062-2073.
- [67] Y.F. Shen, H. Zhang, J.Q. Zhang, C.Y. Tian, Y.A. Shi, D.D. Qiu, Z.Q. Zhang, K. Lu, Z.X. Wei, In Situ Absorption Characterization Guided Slot-Die-Coated High-Performance Large-Area Flexible Organic Solar Cells and Modules, *Adv. Mater.* (2022) 9.
- [68] T.J. Fauvell, T.Y. Zheng, N.E. Jackson, M.A. Ratner, L.P. Yu, L.X. Chen, Photophysical and Morphological Implications of Single-Strand Conjugated Polymer Folding in Solution, *Chem. Mater.* 28(8) (2016) 2814-2822.
- [69] J.G. Liu, L. Chen, B.R. Gao, X.X. Cao, Y.C. Han, Z.Y. Xie, L.X. Wang, Constructing the nanointerpenetrating structure of PCDTBT:PC₇₀BM bulk heterojunction solar cells induced by aggregation of PC₇₀BM via mixed-solvent vapor annealing, *J. Mater. Chem. A* 1(20) (2013) 6216-6225.
- [70] J.G. Liu, Q.J. Liang, H.Y. Wang, M.G. Li, Y.C. Han, Z.Y. Xie, L.X. Wang, Improving the Morphology of PCDTBT:PC₇₀BM Bulk Heterojunction by Mixed-Solvent Vapor-Assisted Imprinting: Inhibiting Inter-calculation, Optimizing Vertical Phase Separation, and Enhancing Photon Absorption, *J. Phys. Chem. C* 118(9) (2014) 4585-4595.
- [71] R. Zhang, H. Yang, K. Zhou, J.D. Zhang, J.G. Liu, X.H. Yu, R.B. Xing, Y.C. Han, Optimized Domain Size and Enlarged D/A Interface by Tuning Intermolecular Interaction in All-Polymer Ternary Solar Cells, *J. Polym. Sci. Pt. B-Polym. Phys.* 54(18) (2016) 1811-1819.
- [72] N.S. Güldal, T. Kassar, M. Berlinghof, T. Unruh, C.J. Brabec, In situ characterization methods for evaluating microstructure formation and drying kinetics of solution-processed organic bulk-heterojunction films, *J. Mater. Res.* 32(10) (2017) 1855-1879.

- [73] Y. Liu, A. Yangui, R. Zhang, A. Kiligaridis, E. Moons, F. Gao, O. Ingnas, I.G. Scheblykin, F. Zhang, In Situ Optical Studies on Morphology Formation in Organic Photovoltaic Blends, *Small Methods* 5(10) (2021) e2100585.
- [74] S. Engmann, F.A. Bokel, H.W. Ro, D.M. DeLongchamp, L.J. Richter, Real-Time Photoluminescence Studies of Structure Evolution in Organic Solar Cells, *Adv. Energy Mater.* 6(10) (2016) 12.
- [75] W.Y. Huang, P.T. Huang, Y.K. Han, C.C. Lee, T.L. Hsieh, M.Y. Chang, Aggregation and Gelation Effects on the Performance of Poly(3-hexylthiophene)/Fullerene Solar Cells, *Macromolecules* 41(20) (2008) 7485-7489.
- [76] W.R. Wu, U.S. Jeng, C.J. Su, K.H. Wei, M.S. Su, M.Y. Chiu, C.Y. Chen, W.B. Su, C.H. Su, A.C. Su, Competition between Fullerene Aggregation and Poly(3-hexylthiophene) Crystallization upon Annealing of Bulk Heterojunction Solar Cells, *ACS Nano* 5(8) (2011) 6233-6243.
- [77] C.H. Zhang, A. Mumyatov, S. Langner, J.D. Perea, T. Kassar, J. Min, L.L. Ke, H.W. Chen, K.L. Gerasimov, D.V. Anokhin, D.A. Ivanov, T. Ameri, A. Osvet, D.K. Susarova, T. Unruh, N. Li, P. Troshin, C.J. Brabec, Overcoming the Thermal Instability of Efficient Polymer Solar Cells by Employing Novel Fullerene-Based Acceptors, *Adv. Energy Mater.* 7(3) (2017) 8.
- [78] J.D. Roehling, D. Baran, J. Sit, T. Kassar, T. Ameri, T. Unruh, C.J. Brabec, A.J. Moule, Nanoscale Morphology of PTB7 Based Organic Photovoltaics as a Function of Fullerene Size, *Sci. Rep.* 6 (2016) 12.
- [79] L.A. Perez, K.W. Chou, J.A. Love, T.S. van der Poll, D.M. Smilgies, T.Q. Nguyen, E.J. Kramer, A. Amassian, G.C. Bazan, Solvent Additive Effects on Small Molecule Crystallization in Bulk Heterojunction Solar Cells Probed During Spin Casting, *Adv. Mater.* 25(44) (2013) 6380-6384.
- [80] F. Liu, S. Ferdous, E. Schaible, A. Hexemer, M. Church, X.D. Ding, C. Wang, T.P. Russell, Fast Printing and In Situ Morphology Observation of Organic Photovoltaics Using Slot-Die Coating, *Adv. Mater.* 27(5) (2015) 886-891.
- [81] W.R. Wu, C.J. Su, W.T. Chuang, Y.C. Huang, P.W. Yang, P.C. Lin, C.Y. Chen, T.Y. Yang, A.C. Su, K.H. Wei, C.M. Liu, U.S. Jeng, Surface Layering and Supersaturation for Top-Down Nanostructural Development during Spin Coating of Polymer/Fullerene Thin Films, *Adv. Energy Mater.* 7(14) (2017) 11.
- [82] O. Wodo, B. Ganapathysubramanian, Modeling morphology evolution during solvent-based fabrication of organic solar cells, *Comput. Mater. Sci.* 55 (2012) 113-126.
- [83] J.W.P. Schmelzer, Crystal nucleation and growth in glass-forming melts: Experiment and theory, *J. Non-Cryst. Solids* 354(2-9) (2008) 269-278.
- [84] L. Cormier, Nucleation in Glasses-New Experimental Findings and Recent Theories, PMS. (2014).
- [85] A.D. de Zerio, C. Muller, Glass Forming Acceptor Alloys for Highly Efficient and Thermally Stable Ternary Organic Solar Cells, *Adv. Energy Mater.* 8(28) (2018) 18.
- [86] Z.N. Gerek, J.R. Elliott, Self-Diffusivity Estimation by Molecular Dynamics, *Ind. Eng. Chem. Res.* 49(7) (2010) 3411-3423.
- [87] V.M. Fokin, J.W.P. Schmelzer, M.L.F. Nascimento, E.D. Zanotto, Diffusion coefficients for crystal nucleation and growth in deeply undercooled glass-forming liquids, *J. Chem. Phys.* 126(23) (2007) 6.
- [88] Y. Yue, B. Zheng, W. Yang, L. Huo, J. Wang, L. Jiang, Meniscus-Assisted Coating with Optimized Active-Layer Morphology toward Highly Efficient All-Polymer Solar Cells, *Adv. Mater.* 34(14) (2022) e2108508.
- [89] J.J. van Franeker, D. Hermida-Merino, C. Gommès, K. Arapov, J.J. Michels, R.A.J. Janssen, G. Portale, Sub-Micrometer Structure Formation during Spin Coating Revealed by Time-Resolved In Situ Laser and X-Ray Scattering, *Adv. Funct. Mater.* 27(46) (2017) 12.

- [90] Y. Wang, X. Wang, B. Lin, Z. Bi, X. Zhou, H.B. Naveed, K. Zhou, H. Yan, Z. Tang, W. Ma, Achieving Balanced Crystallization Kinetics of Donor and Acceptor by Sequential-Blade Coated Double Bulk Heterojunction Organic Solar Cells, *Adv. Energy Mater.* 10(28) (2020).
- [91] H. Zhao, B.J. Lin, J.W. Xue, H.B. Naveed, C. Zhao, X.B. Zhou, K. Zhou, H.B. Wu, Y.H. Cai, D.Q. Yun, Z. Tang, W. Ma, Kinetics Manipulation Enables High-Performance Thick Ternary Organic Solar Cells via R2R-Compatible Slot-Die Coating, *Adv. Mater.* 34(7) (2022) 10.
- [92] P.G.V. Sampaio, M.O.A. González, P.D. Ferreira, P.D.J. Vidal, J.P.P. Pereira, H.R. Ferreira, P.C. Oprime, Overview of printing and coating techniques in the production of organic photovoltaic cells, *Int. J. Energy Res.* 44(13) (2020) 9912-9931.
- [93] J.Q. Xu, J.Z. Zhan, G.Q. Zhou, W.K. Zhong, M. Zhang, X.N. Xue, L. Zhu, S.F. Leng, J.J. Chen, Y.C. Zou, X. Su, Z.W. Shi, H.M. Zhu, M.J. Zhang, C.C. Chen, Y.F. Li, Y.M. Zhang, F. Liu, Slot-Die-Coated Organic Solar Cells Optimized through Multistep Crystallization Kinetics, *Solar RRL* 6(6) (2022) 11.
- [94] M. Reichenberger, D. Kroh, G.M.M. Matrone, K. Schotz, S. Proller, O. Filonik, M.E. Thordardottir, E.M. Herzig, H. Bassler, N. Stingelin, A. Kohler, Controlling aggregate formation in conjugated polymers by spin-coating below the critical temperature of the disorder-order transition, *J. Polym. Sci. Pt. B-Polym. Phys.* 56(6) (2018) 532-542.
- [95] X. Zhang, H. Zhang, S.L. Li, L.E. Xiao, S.W. Zhang, B. Han, J.J. Kang, H.Q. Zhou, Development and application of blade-coating technique in organic solar cells, *Nano Res.* (2023) 18.
- [96] Z.X. Peng, Y.W. Zhang, X.K. Sun, W.C. Zhao, F.G. Bian, Y.H. Geng, L. Ye, C.M. Yang, Real-Time Probing and Unraveling the Morphology Formation of Blade-Coated Ternary Nonfullerene Organic Photovoltaics with In Situ X-Ray Scattering, *Adv. Funct. Mater.* 33(14) (2023) 10.
- [97] M. Le Berre, Y. Chen, D. Baigl, From Convective Assembly to Landau-Levich Deposition of Multilayered Phospholipid Films of Controlled Thickness, *Langmuir* 25(5) (2009) 2554-2557.
- [98] J. Yuan, D.J. Liu, H. Zhao, B.J. Lin, X.B. Zhou, H.B. Naveed, C. Zhao, K. Zhou, Z. Tang, F. Chen, W. Ma, Patterned Blade Coating Strategy Enables the Enhanced Device Reproducibility and Optimized Morphology of Organic Solar Cells, *Adv. Energy Mater.* 11(18) (2021) 10.
- [99] Y. Zhao, G. Wang, Y. Wang, T. Xiao, M.A. Adil, G. Lu, J. Zhang, Z. Wei, A Sequential Slot-Die Coated Ternary System Enables Efficient Flexible Organic Solar Cells, *Solar RRL* 3(3) (2019) 9.
- [100] S.K. Bhattacharya, K.S. Moon, R.R. Tummala, G.S. May, Meniscus coating: A low-cost polymer deposition method for system-on-package (SOP) substrates, *IEEE Trans. Electron. Packag. Manuf.* 26(2) (2003) 110-114.
- [101] T. Ghos, O. Malinkiewicz, B. Conings, L. Lutsen, D.J. Vanderzande, H.J. Bolink, W. Maes, Solution-processed bi-layer polythiophene-fullerene organic solar cells, *RSC Adv.* 3(47) (2013) 25197-25203.
- [102] X.Z. Dai, Y.H. Deng, C.H. Van Brackle, J.S. Huang, Meniscus fabrication of halide perovskite thin films at high throughput for large area and low-cost solar panels, *Int. J. Extreme Manuf.* 1(2) (2019) 14.
- [103] F.C. Krebs, Fabrication and processing of polymer solar cells: A review of printing and coating techniques, *Sol. Energy Mater. Sol. Cells* 93(4) (2009) 394-412.
- [104] L. Zhu, W. Zhong, C. Qiu, B. Lyu, Z. Zhou, M. Zhang, J. Song, J. Xu, J. Wang, J. Ali, W. Feng, Z. Shi, X. Gu, L. Ying, Y. Zhang, F. Liu, Aggregation-Induced Multilength Scaled Morphology Enabling 11.76% Efficiency in All-Polymer Solar Cells Using Printing Fabrication, *Adv. Mater.* 31(41) (2019) e1902899.
- [105] Y. Sun, J.-g. Liu, Y. Ding, Y.-c. Han, Controlling the surface composition of PCBM in P3HT/PCBM blend films by using mixed solvents with different evaporation rates, *Chinese J Polym Sci.* 31(7) (2013) 1029-1037.

- [106] X. Jiang, P. Chotard, K. Luo, F. Eckmann, S. Tu, M.A. Reus, S. Yin, J. Reitenbach, C.L. Weindl, M. Schwartzkopf, S.V. Roth, P. Müller-Buschbaum, Revealing Donor-Acceptor Interaction on the Printed Active Layer Morphology and the Formation Kinetics for Nonfullerene Organic Solar Cells at Ambient Conditions, *Adv. Energy Mater.* 12(14) (2022).
- [107] K. Zhou, R. Zhang, J. Liu, M. Li, X. Yu, R. Xing, Y. Han, Donor/Acceptor Molecular Orientation-Dependent Photovoltaic Performance in All-Polymer Solar Cells, *ACS Appl. Mater. Interfaces.* 7(45) (2015) 25352-61.
- [108] R. Zhang, Y. Yan, Q. Zhang, Q. Liang, J. Zhang, X. Yu, J. Liu, Y. Han, To Reveal the Importance of the Crystallization Sequence on Micro-Morphological Structures of All-Crystalline Polymer Blends by In Situ Investigation, *ACS Appl. Mater. Interfaces.* 13(18) (2021) 21756-21764.
- [109] H. Zhao, H.B. Naveed, B. Lin, X. Zhou, J. Yuan, K. Zhou, H. Wu, R. Guo, M.A. Scheel, A. Chumakov, S.V. Roth, Z. Tang, P. Muller-Buschbaum, W. Ma, Hot Hydrocarbon-Solvent Slot-Die Coating Enables High-Efficiency Organic Solar Cells with Temperature-Dependent Aggregation Behavior, *Adv. Mater.* 32(39) (2020) e2002302.
- [110] J.Y. Oh, M. Shin, T.I. Lee, W.S. Jang, Y. Min, J.-M. Myoung, H.K. Baik, U. Jeong, Self-Seeded Growth of Poly(3-hexylthiophene) (P3HT) Nanofibrils by a Cycle of Cooling and Heating in Solutions, *Macromolecules* 45(18) (2012) 7504-7513.
- [111] L. Ye, Y. Xie, K. Weng, H.S. Ryu, C. Li, Y. Cai, H. Fu, D. Wei, H.Y. Woo, S. Tan, Y. Sun, Insertion of chlorine atoms onto π -bridges of conjugated polymer enables improved photovoltaic performance, *Nano Energy* 58 (2019) 220-226.
- [112] Q. Liang, Y. Chang, C. Liang, H. Zhu, Z. Guo, J. Liu, Application of Crystallization Kinetics Strategy in Morphology Control of Solar Cells Based on Nonfullerene Blends, *Acta Phys.-Chim. Sin.* (2023), 2212006.
- [113] K. Zhou, Q. Zhao, R. Zhang, X. Cao, X. Yu, J. Liu, Y. Han, Decreased domain size of *p* - DTS(FBTTh₂)₂/P(NDI2OD-T2) blend films due to their different solution aggregation behavior at different temperatures, *Phys. Chem. Chem. Phys.* 19(48) (2017) 32373-32380.
- [114] J.Y. Yuan, Y.L. Xu, G.Z. Shi, X.F. Ling, L. Ying, F. Huang, T.H. Lee, H.Y. Woo, J.Y. Kim, Y. Cao, W.L. Ma, Engineering the morphology via processing additives in multiple all-polymer solar cells for improved performance, *J. Mater. Chem. A* 6(22) (2018) 10421-10432.
- [115] Y. Yao, J.H. Hou, Z. Xu, G. Li, Y. Yang, Effect of solvent mixture on the nanoscale phase separation in polymer solar cells, *Adv. Funct. Mater.* 18(12) (2008) 1783-1789.
- [116] J.C. Hummelen, C.J. Brabec, F. Padinger, N.S. Sariciftci, Photovoltaic Properties Of Conjugated Polymer/methanofullerene Composites Embedded In A Polystyrene Matrix, *J. Appl. Phys.* 85(9) (1999) 6866-6872.
- [117] J. Zhan, L. Wang, M. Zhang, L. Zhu, T. Hao, G. Zhou, Z. Zhou, J. Chen, W. Zhong, C. Qiu, S. Leng, Y. Zou, Z. Shi, H. Zhu, W. Feng, M. Zhang, Y. Li, Y. Zhang, F. Liu, Manipulating Crystallization Kinetics of Conjugated Polymers in Nonfullerene Photovoltaic Blends toward Refined Morphologies and Higher Performances, *Macromolecules* 54(9) (2021) 4030-4041.
- [118] J.L. Hernandez, N. Deb, R.M.W. Wolfe, C.K. Lo, S. Engmann, L.J. Richter, J.R. Reynolds, Simple transfer from spin coating to blade coating through processing aggregated solutions, *J. Mater. Chem. A* 5(39) (2017) 20687-20695.
- [119] E.F. Manley, J. Strzalka, T.J. Fauvell, N.E. Jackson, M.J. Leonardi, N.D. Eastham, T.J. Marks, L.X. Chen, In Situ GIWAXS Analysis of Solvent and Additive Effects on PTB7 Thin Film Microstructure Evolution during Spin, *Adv. Mater.* 29(43) (2017) 9.

- [120] J.G. Liu, S.Y. Zeng, Z.G. Zhang, J. Peng, Q.J. Liang, Optimizing the Phase-Separated Domain Size of the Active Layer via Sequential Crystallization in All-Polymer Solar Cells, *J. Phys. Chem. Lett.* 11(6) (2020) 2314-2321.
- [121] Q. Liang, X. Jiao, Y. Yan, Z. Xie, G. Lu, J. Liu, Y. Han, Separating Crystallization Process of P3HT and O-IDTBR to Construct Highly Crystalline Interpenetrating Network with Optimized Vertical Phase Separation, *Adv. Funct. Mater.* 29(47) (2019).
- [122] C.J. Brabec, H. Johannson, F. Padinger, H. Neugebauer, J.C. Hummelen, N.S. Sariciftci, Photoinduced FT-IR spectroscopy and CW-photocurrent measurements of conjugated polymers and fullerenes blended into a conventional polymer matrix, *Sol. Energy Mater Sol. Cells* 61(1) (2000) 19-33.
- [123] N. Camaioni, M. Catellani, S. Luzzati, A. Migliori, Morphological characterization of poly(3-octylthiophene):plasticizer:C60 blends, *Thin Solid Films* 403 (2002) 489-494.
- [124] H. Guan, Q.G. Liao, T.H. Huang, S. Geng, Z.L. Cao, Z.L. Zhang, D.J. Wang, J. Zhang, Solid Additive Enables Organic Solar Cells with Efficiency up to 18.6%, *ACS Appl. Mater. Interfaces* 15(21) (2023) 25774-25782.
- [125] P. Fan, W.J. Sun, X.H. Zhang, Y. Wu, Q. Hu, Q. Zhang, J.S. Yu, T.P. Russell, Bifunctional Bis-benzophenone as A Solid Additive for Non-Fullerene Solar Cells, *Adv. Funct. Mater.* 31(8) (2021) 7.
- [126] Y. Yan, Y.D. Liu, J.D. Zhang, Q. Zhang, Y.C. Han, Optimization of local orientation and vertical phase separation by adding a volatilizable solid additive to the J51:N2200 blend to improve its photovoltaic performance, *J. Mater. Chem. C* 9(11) (2021) 3835-3845.
- [127] H.J. Bin, Z.G. Zhang, L. Gao, S.S. Chen, L. Zhong, L.W. Xue, C. Yang, Y.F. Li, Non-Fullerene Polymer Solar Cells Based on Alkylthio and Fluorine Substituted 2D-Conjugated Polymers Reach 9.5% Efficiency, *J. Am. Chem. Soc.* 138(13) (2016) 4657-4664.
- [128] J.F. Ge, L. Hong, W. Song, L. Xie, J.S. Zhang, Z.Y. Chen, K.B. Yu, R.X. Peng, X.L. Zhang, Z.Y. Ge, Solvent Annealing Enables 15.39% Efficiency All-Small-Molecule Solar Cells through Improved Molecule Interconnection and Reduced Non-Radiative Loss, *Adv. Energy Mater.* 11(22) (2021) 9.
- [129] G. Li, V. Shrotriya, J.S. Huang, Y. Yao, T. Moriarty, K. Emery, Y. Yang, High-efficiency solution processable polymer photovoltaic cells by self-organization of polymer blends, *Nat. Mater.* 4(11) (2005) 864-868.
- [130] G. Li, V. Shrotriya, Y. Yao, Y. Yang, Investigation of annealing effects and film thickness dependence of polymer solar cells based on poly(3-hexylthiophene), *J. Appl. Phys.* 98(4) (2005) 5.
- [131] J. Min, N.S. Guldal, J. Guo, C. Fang, X.C. Jiao, H.W. Hu, T. Heumuller, H. Ade, C.J. Brabec, Gaining further insight into the effects of thermal annealing and solvent vapor annealing on time morphological development and degradation in small molecule solar cells, *J. Mater. Chem. A* 5(34) (2017) 18101-18110.
- [132] J. Guo, H.J. Bin, W. Wang, B.C. Chen, J. Guo, R. Sun, Z.G. Zhang, X.C. Jiao, Y.F. Li, J. Min, All-small molecule solar cells based on donor molecule optimization with highly enhanced efficiency and stability, *J. Mater. Chem. A* 6(32) (2018) 15675-15683.
- [133] W. Ma, C. Yang, X. Gong, K. Lee, A.J. Heeger, Thermally Stable, Efficient Polymer Solar Cells with Nanoscale Control of the Interpenetrating Network Morphology, *Adv. Funct. Mater.* (10) (2005) 15.
- [134] X. Cheng, M. Li, Z. Liang, M. Gao, L. Ye, Y. Geng, Implications of Crystallization Temperatures of Organic Small Molecules in Optimizing Nonfullerene Solar Cell Performance, *ACS Appl. Energy Mater.* 4(8) (2021) 8442-8453.
- [135] X. Zhang, P. Fan, Z. Wang, D. Zheng, J. Yu, Morphology Regulation by Upside-Down Thermal Annealing Based on Blend Thick-Film Organic Solar Cells, *J. Phys. Chem. C* 125(28) (2021) 15194-15199.

- [136] A. Levitsky, S.A. Schneider, E. Rabkin, M.F. Toney, G.L. Frey, Bridging the thermodynamics and kinetics of temperature-induced morphology evolution in polymer/fullerene organic solar cell bulk heterojunction, *Mater. Horizons* 8(4) (2021) 1272-1285.
- [137] C. Jin, B.C. Olsen, E.J. Lubber, J.M. Buriak, Nanopatterning via Solvent Vapor Annealing of Block Copolymer Thin Films, *Chem. Mater.* 29(1) (2017) 176-188.
- [138] K. Sun, Z. Xiao, E. Hanssen, M.F.G. Klein, H.H. Dam, M. Pfaff, D. Gerthsen, W.W.H. Wong, D.J. Jones, The role of solvent vapor annealing in highly efficient air-processed small molecule solar cells, *J. Mater. Chem. A* 2(24) (2014) 9048-9054.
- [139] M. Babics, R.Z. Liang, K. Wang, F. Cruciani, Z.P. Kan, M. Wohlfahrt, M.C. Tang, F. Laquai, P.M. Beaujuge, Solvent Vapor Annealing-Mediated Crystallization Directs Charge Generation, Recombination and Extraction in BHJ Solar Cells, *Chem. Mater.* 30(3) (2018) 789-798.
- [140] C. Harreiß, S. Langner, M. Wu, M. Berlinghof, S. Rechberger, J. Will, M. Conroy, U. Bangert, T. Unruh, C.J. Brabec, E. Spiecker, Understanding and Controlling the Evolution of Nanomorphology and Crystallinity of Organic Bulk-Heterojunction Blends with Solvent Vapor Annealing, *Solar RRL* 6(9) (2022).
- [141] J. Liu, L. Chen, B. Gao, X. Cao, Y. Han, Z. Xie, L. Wang, Constructing the nanointerpenetrating structure of PCDTBT:PC70BM bulk heterojunction solar cells induced by aggregation of PC₇₀BM via mixed-solvent vapor annealing, *J. Mater. Chem. A* 1(20) (2013) 6216-6225.
- [142] Q. Liang, J. Han, C. Song, X. Yu, D.-M. Smilgies, K. Zhao, J. Liu, Y. Han, Reducing the confinement of PBDB-T to ITIC to improve the crystallinity of PBDB-T/ITIC blends, *J. Mater. Chem. A* 6(32) (2018) 15610-15620.
- [143] Y. Zhao, Z. Xie, Y. Qu, Y. Geng, L. Wang, Solvent-vapor treatment induced performance enhancement of poly(3-hexylthiophene):methanofullerene bulk-heterojunction photovoltaic cells, *Appl. Phys. Lett.* 90(4) (2007) 15.